PROC. IMECHE-*PART E*-

JOURNAL OF PROCESS MECHANICAL ENGINEERING

eISSN: 20413009 | ISSN: 09544089

Impact Factor: 1.448

PUBLISHER: SAGE PUBLISHING

Accepted September 20th 2017

OSCILLATORY DISSIPATIVE CONJUGATE HEAT AND MASS TRANSFER IN CHEMICALLY-REACTING MICROPOLAR FLOW WITH WALL COUPLE STRESS: *FINITE ELEMENT NUMERICAL STUDY*

Shamshuddin MD [1*], Siva Reddy Sheri[2] and O. Anwar Bég[3]

[1*]*Department of Mathematics, Vaagdevi College of Engineering, Warangal, Telangana,* ***India.***
[2]*Department of Mathematics, GITAM University, Hyderabad Campus, Telangana,* ***India****.*
[3]*Fluid Mechanics and Propulsion, Aeronautical and Mechanical Engineering, University of Salford, Newton Building, The Crescent, Salford, M54WT, England,* ***UK.***
*******Corresponding author:* shammaths@gmail.com

Abstract

High temperature non-Newtonian materials processing provides a stimulating area for process engineering simulation. Motivated by emerging applications in this area, the present article investigates *the time-dependent free convective flow of a chemically-reacting micropolar fluid from a vertical plate oscillating in its own plane adjacent to a porous medium*. Thermal radiative, viscous dissipation and wall couple stress effects are included. The Rosseland diffusion approximation is used to model uni-directional radiative heat flux in the energy equation. Darcy's model is adopted to mimic porous medium drag force effects. The governing two-dimensional conservation equations are normalized with appropriate variables and transformed into a dimensionless, coupled, nonlinear system of partial differential equations under the assumption of low Reynolds number. The governing boundary value problem is then solved under physically viable boundary conditions numerically with a finite element method based on the weighted residual approach. Graphical illustrations for velocity, micro-rotation (angular velocity), temperature and concentration are obtained as functions of the emerging physical parameters i.e. thermal radiation, viscous dissipation, first order chemical reaction parameter etc. Furthermore, friction factor (skin friction), surface heat transfer and mass transfer rates have been tabulated quantitatively for selected thermo-physical parameters. A comparison with previously published paper is made to check the validity and accuracy of the present finite element solutions under some limiting cases and excellent agreement is attained. Additionally, a mesh independence study is conducted. The model is relevant to reactive polymeric materials processing simulation.

Keywords *Wall couple stress, Thermal Radiation, Chemical reaction, Micropolar fluid, FEM, Materials processing, Buoyancy.*

1. INTRODUCTION

In recent years, non-Newtonian fluids have received significance interest, since they offer a more accurate framework for simulating the characteristics of a fluid with suspended particles than the classical Navier-Stokes (Newtonian) viscous model. Such fluids abound in complex industrial processes for example, in slurry and petro-chemical materials processing. Micro-structural fluids require additional balance equations corresponding to angular momentum. Eringen [1] proposed the theory of micropolar fluids (a simplification of his more complex micromorphic fluid model) by developing constitute equations that take into account the effects arising from the local structure and micro-motions of the micro elements. Also micropolar fluids can support the shear stress, couple stress, body couples and exhibit gyratory motions. By generalizing of micropolar fluids to heat conduction and other thermal effects, Eringen [2] developed a robust theory of thermo-micropolar fluids. These theories present an excellent mechanism for exploring new non-Newtonian characteristics and simultaneously validating solutions to mathematical models. Interesting aspects of theory and applications of micropolar fluids can be found in books by Eringen [3] and Lukaswiascz [4]. Further details of applications in petro-chemical and process engineering are provided in the lucid review article of Airman *et al*. [5]. These investigations have addressed numerous multi-physical phenomena including thermal dispersion, thermal radiation, electrophoresis, wavy surfaces, body rotations, oscillatory flow, squeezing hydrodynamics, fluid dynamic stability and magnetohydrodynamics. The multi-scale, multi-physical nature of materials processing systems therefore provides a rich arena for exploring micropolar transport phenomena. Recent investigations of micropolar materials processing include Gupta *et al*. [6] who used a variational finite element method to investigate free and forced convection of micropolar liquids in contracting sheet flow under strong radiative flux. Rahman and Sultana [7] analyzed the radiative heat transfer effects on micropolar flow with variable heat flux in a porous medium was examined by Considering the effects of MHD and radiation Reddy [8] investigated unsteady convection flow of micropolar fluid past a vertical porous plate with variable wall heat flux. Zueco *et al.* [9] used network electro-thermal simulation to analyze buoyancy-driven magnetic micropolar convection flows in vertical conduits containing complex porous materials.

Conjugate heat and mass transfer problems have also stimulated considerable interest. Both numerical and analytical studies have ben communicated in this regard. This category of flow occurs as a result of combined buoyancy effects of thermal diffusion and diffusion through chemical species, which find important applications in industrial materials fabrication and chemical engineering. These include food drying, foodstuff processing and polymer production. The term conjugate heat transfer describes the interaction between the convective fluid and heat conduction through the bounding wall. The heat transfer coefficient or thermal boundary conditions become an integral part of solving such problems which deviate from the conventional boundary layer flow analysis, in which they are usually specified. This condition is necessary in the heat transfer analysis of extended surfaces where the thermal boundary conditions are specified only at the ends of the surfaces. It may be noted that conjugate/convective thermal boundary conditions are known arise in many diverse areas of technology including combustion in gas turbines, convective flows setup where the bounding surfaces absorb heat by solar radiation, design of efficient heat exchangers, optimization of turbine blade cooling system etc. An important analysis in this regard was presented by Aziz [10] who considered convective surface boundary conditions. This in turn has stimulated a number of investigations in boundary layer flows with convective surface boundary conditions for different physical scenarios. By employing finite difference schemes, Pop and Merkin [11, 12] studied conjugate heat transfer from a vertical plate in a saturated permeable medium. Conjugate forced convection heat transfer from a continuous and moving flat sheet was analyzed by Char *et al.*, [13] employing a cubic spline collocation numerical method. Recently Khalid *et al.* [14] presented exact solutions (using a Laplace transform method) for conjugate heat and mass transfer in transient micropolar flow with wall couple stress. This has partly motivated the current investigation in which we extend the analysis in [14] to consider thermal radiation, viscous dissipation and first order chemical reaction effects, all of which may feature in realistic materials and process flow systems. Furthermore, detailed reviews of other investigations into conjugate heat transfer are provided by Chaudhary and Jain [15], Hussain [16], Zhang [17] and Bejan [18]. In recent years, conjugate natural convection flows with radiative heat transfer have mobilized some interest owing their significance in high-temperature engineering systems such as heat exchangers, combustion chambers and materials synthesis. These flows require a more sophisticated approach to radiative heat transfer in the system which can substantially influence

performance and modify characteristics of manufactured products. In addition to this, such regimes are strongly influenced by thermal boundary conditions. Arpaci [19] conducted seminal work on analyzing thermal radiation effects in laminar free convection from a heated vertical plate. England and Emery [20] computed the impact of thermal radiation of an optically-thin gray gas on the laminar free convection flow past a stationary vertical plate. Thereafter many researchers further studied thermal radiation problems in fluid dynamics including Özisik [21] who considered the interaction of thermal radiation transfer with both thermal conduction and convection. Bestman and Adjepong [22] presented an analysis on unsteady hydromagnetic free convection flow with radiative heat transfer in a rotating fluid. Other studies of relevance include convection-radiation flow along a vertical wavy surface as examined by Molla and Hossain [23]. Jang *et al.* [24] studied flows in rotating horizontal rectangular ducts with radiation effects. Jang *et al*. [25] further investigated radiative flows in stationary rectangular ducts. Free convective transport along an inclined flat plate with temperature-dependent viscosity was studied by Siddiqa *et al.* [26]. Siddiqa and Hossain [27] investigated mixed convection with radiative flux effects. In the context of *micropolar flows,* several researchers have also examined thermal radiative heat transfer. Abo-Eldahab and Ghonaim [28] evaluated radiation effects on heat transfer of a micropolar fluid through a porous medium. Olajuwon and Oahimire [29] obtained perturbation solutions for the double-diffusive convection in time-dependent radiative hydromagnetic micropolar convection. Kundu *et al*. [30] studied thermo-diffusive and radiative effects on rotating micropolar convection flows.

In the most of the above investigations, viscous heating has generally been neglected on the premise that under normal conditions the Eckert number is small based on an order of magnitude analysis. The viscous dissipation effect however can have a significant influence in materials processing operations, in particular those associated with rheological (non-Newtonian) processes, as elaborated by Warren [31]. Chen [32] described the effects of heat and mass transfer in MHD free convection with Ohmic heating and viscous dissipation. Gnaneswara and Bhaskar [33] investigated the radiation and mass transfer effects on transient magneto-convection with viscous dissipation.

In numerous process engineering systems, *chemical reactions* take place. These can markedly modify heat and mass transfer rates. Most analytical studies consider first order chemical reaction effects and assume the reaction to be destructive. Recently Srinivasacharya and Upender

[34] have considered the composite effects of thermal radiation and chemical reaction on magnetic free convection heat and mass transfer in micropolar fluids. Sheri and Shamshuddin MD [35] have addressed the problem of coupled heat and mass transfer in magnetohydrodynamic micropolar flow with both viscous dissipation and chemical reaction effects. Sheri and Shamshuddin [36] have further presented finite element numerical solutions for diffuso-thermal and chemical reaction effects on transient free convection micropolar flow. Further studies of *reactive micropolar flows* include Rawat *et al*. [37] (which considered double diffusive convection in reactive micropolar flow from an extending sheet) and Pal and Talukdar [38].

The presence of *oscillatory flow* in materials fabrication processes is also of great importance. This invokes time-dependent effects and these can dramatically modify momentum, heat and species diffusion characteristics, as elaborated by Reis [39]. Many insightful investigations have been reported concerning oscillatory transport phenomena. These include Pan and Li [40], Adesanya *et al.* [41], Bhargava *et al.* [42] (who used finite element methods and considered cross-diffusion), Adesanya [43] who considered momentum slip effects at the wall and Rajesh et al. [44] who considered hydromagnetic enrobing flow over a curved geometry with reactive and thermal oscillation behavior. Further studies include Adesanya *et al.* [45] who considered viscous heating in pulsatile porous media pumping, Maqbool *et al*. [46] who presented Fourier solutions to a family of oscillatory non-Newtonian ferromagnetic gel flows, Adesanya *et al.* [47] who considered transient boundary conditions in magnetic heat transfer and Bég *et al.* [48] who developed network electro-thermal solutions for oscillatory heat transfer of magnetized polymers in a spinning channel.

The above oscillatory studies all confirmed the considerable impact that oscillation frequency exerts on shear stress, wall heat transfer rates and in some cases [46] also on vorticity fields. However they did not consider species diffusion or the micropolar model. In the present problem, therefore, we extended the analytical work of Khalid *et al.* [14] by taking into account of *thermal radiation, viscous dissipation and first order chemical reaction effects* and deriving finite element numerical solutions for *generalized micropolar radiative-convection flow from a vertical surface in a porous medium*. The closed-form exponential solutions presented by Khalid *et al.* [14] provide a benchmark for the current computational solutions. The effects of various emerging thermo-physical parameters on the velocity, micro-rotation velocity, temperature and

concentration profiles as well as on local skin friction coefficient and wall couple stress are visualized and tabulated. Furthermore, a mesh-independence study is also conducted. The current problem, to the best knowledge of the authors, has not been communicated thusfar in the technical literature.

2. MATHEMATICAL MODEL

Consider the unsteady, laminar incompressible, free convective heat and mass transfer flow of micropolar fluid from an infinite porous oscillating vertical plate adjacent to a porous medium. Thermal radiation, viscous dissipation and chemical reaction effects are included. The coordinate system is such that the x' axis is taken along the plate and y' axis is taken perpendicular to the plate. The micropolar fluid saturates the porous half space $y' > 0$. The schematic model of the coordinate system and physical model is represented in **Figure 1**. Initially at the time $t' = 0$, both the fluid and the plate are at rest with constant temperature T'_∞ and constant concentration C'_∞. At time $t' > 0$ the plate is given sudden impulse, and the motion is induced against gravity such that plate begins to oscillate in its own plane with velocity $V = U\ H(t')\ Cos\ (\alpha t')\vec{i}$ .Here $H(t')$ is the Heaviside (unit step) function, U is the amplitude of the motion, $\vec{i}$ is the unit vector in the vertical flow direction and α is the frequency of oscillation. The temperature T_w and concentration C_w of the plate are raised linearly with respect to time and thereafter maintained as constant. It is assumed that the plate is infinite in extent and hence all physical quantities depend on y' and t' only. By virtue of these assumptions the governing equations for unsteady natural convective flow under Boussinesq's approximations may be formulated as follows, by extending the model of Khalid *et al.* [14] to include the radiative flux and porous media terms in Rahman and Sultana [7], the viscous dissipation term in the model of Zueco *et al.* [9] and Reddy *et al.* [33] and the chemical reaction term in the model of Srinivasacharya and Upender [34] we arrive at the new generalized model:

The linear momentum equation:

$$\frac{\partial u'}{\partial t'} = \left(\nu + \frac{K}{\rho}\right)\frac{\partial^2 u'}{\partial y'^2} + g^*\beta_f\left(T'_w - T'_\infty\right) + g^*\beta_C\left(C'_w - C'_\infty\right) + \frac{K}{\rho}\frac{\partial \omega'}{\partial y'} \tag{1}$$

The angular momentum equation:

$$\rho\, j'\left(\frac{\partial \omega'}{\partial t'}\right) = \gamma_o \frac{\partial^2 \omega'}{\partial y'^2} \tag{2}$$

The energy equation:

$$\rho C_p\left(\frac{\partial T}{\partial t'}\right) = \kappa\left(\frac{\partial^2 T}{\partial y'^2}\right) - \left(\frac{\partial q_r}{\partial y'}\right) + \nu\left(\frac{\partial u'}{\partial y'}\right)^2 \tag{3}$$

The concentration equation:

$$\frac{\partial C}{\partial t'} = D_m\left(\frac{\partial^2 C}{\partial y'^2}\right) - K_r'\left(C_w' - C_\infty'\right) \tag{4}$$

The corresponding initial and boundary conditions are given by :

$$\begin{aligned} t' \le 0 \quad & \{u' = 0,\ \omega' = 0, T' = T_\infty',\ C' = C_\infty' && \text{for all } y' \ge 0 \\ t' > 0 \quad & \left\{\begin{array}{ll} u' = H(t')U\cos(\alpha' t'),\ \omega' = -n\frac{\partial u'}{\partial y'}, T_\infty' = T_w', C_\infty' = C_w' & \text{at } y' = 0 \\ u' \to 0, \omega' \to 0, T' \to T', C' \to C_\infty' & \text{as } y' \to \infty \end{array}\right\} \end{aligned} \tag{5}$$

Where u' is velocity, ω is micro-rotation i.e. angular velocity component (spin direction is in the xy plane, γ_o is spin gradient viscosity, ρ is the density of micropolar fluid, g^* is the acceleration due to gravity, t' is time, β_f and β_C are volumetric coefficient of thermal expansion and concentration expansion, ν is the kinematic viscosity, K/ρ is the kinematic micro-rotation viscosity, j' is the micro inertia per unit mass, T', T_∞' are temperature of fluid at boundary layer and far away from surface. At constant pressure p, C_p is the specific heat, κ is the thermal conductivity, q_r is the heat flux, C', C_∞' are concentration of the solute and far away from surface, $\alpha t'$ is the phase angle and D_m is the molecular diffusivity. Here $0 \le n \le 1$. The case of $n = 0$ indicates $\omega = 0$ at the wall i.e. microelements close to the wall surface are unable to rotate due to presence of concentrated particles at the walls. The case of $n = 1/2$, corresponds to weak concentration of micro elements. For $n = 1$, the flow is turbulent, and this case is not considered in the present simulations. These details are also elucidated in Srinivasacharya and Upendar [49] Following Rahman and Sultana [7] and Magyari and Pantokratoras [50], we adopt the Rosseland approximation for radiative flux q_r in the y' direction which is given by:

$$q_r = \frac{-4\bar{\sigma}}{3\bar{k}} \frac{\partial T'^4}{\partial y'} \tag{6}$$

Here $\bar{\sigma}$ and $\bar{k}$ are the Stefan-Boltzmann constant and mean absorption coefficient respectively. Hence the fluid medium is assumed optically-thick for the present analysis. Eqn. (6) results in a highly nonlinear energy equation in T and it is difficult to obtain a solution. However, researchers have resolved this problem by assuming small temperature differences with in the fluid flow (see [51]-[53]). In this situation, Rosseland's model can be linearized about ambient temperature T'_∞ assuming that the difference in the temperature with in the flow such that T'^4 can be expressed as linear combination of the temperature. Using Taylor's series expansion about T' the expansion of T'^4 can be written as follows, neglecting higher order terms:

$$T'^4 \cong 4T_\infty^3 T - 3T_\infty^4 \tag{7}$$

Differentiating equation (6) w.r.t y' and using (7), we obtain:

$$\frac{\partial q_r}{\partial y'} = -\frac{-16T_\infty^3\bar{\sigma}}{3\bar{k}} \frac{\partial^2 T}{\partial y'^2} \tag{8}$$

Now simply replacing T^3 in Eq. (6) with T_∞^3, Eq. (3) can be expressed as follows:

$$\rho C_p\left(\frac{\partial T}{\partial t'}\right) = \kappa\left(1 + \frac{16\bar{\sigma}}{3\bar{k}\,\kappa} T_\infty^3\right)\frac{\partial^2 T}{\partial y'^2} + \nu\left(\frac{\partial u'}{\partial y'}\right)^2 \tag{9}$$

In order to write the governing equations and boundary conditions in dimensionless form, the following non-dimensional quantities are introduced:

$$\left.\begin{aligned} u' = \frac{u}{U},\ y' = \frac{U}{\nu}y,\ t' = \frac{U^2}{\nu}t,\ \omega' = \frac{\nu}{U^2}\omega, \theta = \frac{T' - T'_\infty}{T'_w - T'_\infty}, \phi = \frac{C' - C_\infty}{C'_w - C'_\infty}, \\ \alpha' = \frac{\nu}{U^2}\alpha,\ J' = \frac{U^2}{\nu^2} j \end{aligned}\right\} \tag{10}$$

Here U represents scale of free stream velocity. Furthermore, the spin gradient viscosity γ_o which connects the coefficient of viscosity and micro-inertia is defined as follows:

$$\gamma_o = \left(\mu + \frac{\Lambda}{2}\right) J' = \mu\, J'\left(1 + \frac{\beta}{2}\right) \quad where \quad \beta = \frac{\Lambda}{\mu} \tag{11}$$

Here β denotes the dimensionless viscosity ratio parameter or microrotation parameter, in which Λ is the *coefficient of gyro-viscosity* (Eringen's vortex viscosity) and J' is the dimensionless micro inertia coefficient. By introducing the non-dimensional quantities in eqns. (10), (11), eqns. (1)-(4) reduce to the following dimensionless form :

$$\frac{\partial u}{\partial t} = (1+\beta)\frac{\partial^2 u}{\partial y^2} + \left(G_r\theta + G_m\phi\right) + \beta\left(\frac{\partial \omega}{\partial y}\right) \tag{12}$$

$$\frac{\partial \omega}{\partial t} = \frac{1}{\eta}\left(\frac{\partial^2 \omega}{\partial y^2}\right) \tag{13}$$

$$\frac{\partial \theta}{\partial t} = \frac{1}{\Pr}(1+N)\frac{\partial^2 \theta}{\partial y^2} + Ec\left(\frac{\partial u}{\partial y}\right)^2 \tag{14}$$

$$\frac{\partial \phi}{\partial t} = \frac{1}{Sc}\left(\frac{\partial^2 \phi}{\partial y^2}\right) - \gamma\,\phi \tag{15}$$

Where $\eta = \frac{\mu\, j}{\gamma_o} = \frac{2}{2+\beta}$ denotes dimensionless spin gradient viscosity parameter, $G_r = \frac{\nu g\left(T_w - T_\infty\right)\beta_T}{U^3}$ denotes the Grashof number, $G_m = \frac{\nu g\left(C_w - C_\infty\right)\beta_C}{U^3}$ is the species (solutal) Grashof number, $P_r = \frac{\mu\, C_p}{\kappa}$ is the Prandtl number, $S_c = \frac{\nu}{D_m}$ denotes Schmidt number, $Ec = \frac{U^2}{C_p\left(T_w - T_\infty\right)}$ is the Eckert (viscous heating) number, $N = \frac{16\bar{\sigma}\, T_\infty^3}{3k\,\bar{k}}$ is radiative-conduction parameter and $\gamma = \frac{K'_r\,\nu}{U^2}$ is the chemical reaction parameter. The boundary conditions (5) are then given by the following dimensionless equations

$$
\begin{array}{ll}
t \le 0 & \{u = 0,\ \omega = 0, T = T_\infty,\ C = C_\infty \qquad\qquad\qquad for\ \ all\ \ y \ge 0 \\
t > 0 & \left\{ \begin{array}{l} u = H(t)\cos(\alpha t), \qquad \omega = -n\dfrac{\partial u}{\partial y}, \quad \theta = 1,\ \phi = 1, \qquad at\ \ y = 0 \\ \qquad u \to 0, \omega \to 0, \theta \to 0, \phi \to 0 \qquad\qquad\qquad as\ y \to \infty \end{array} \right\}
\end{array} \tag{16}
$$

3. NUMERICAL SOLUTIONS WITH FINITE ELEMENT METHOD (FEM)

The finite element method (FEM) is employed to solve the transformed, coupled boundary value problem defined by eqns. (12)-(15) under (16). FEM is the most versatile technique available for engineering analysis and equally adept at handling ordinary or partial differential equations as well as integral equations. The general details of the *variational* finite element method are documented succinctly in Reddy [54] and Bathe [55]. FEM has been applied to study many complex boundary value problems in micropolar fluid mechanics, many of which are considered in Bég *et al.* [56]. Micropolar heat and mass transfer applications also include [57]-[59].The fundamental steps involved in the finite-element analysis of a problem are as follows:

- *Discretization of the infinite fluid domain into finite elements*
- *Derivation of element equations*
- *Assembly of Element Equations*
- *Imposition of boundary conditions*
- *Solution of assembled equations*

The final matrix equation obtained can be solved by any efficient iterative scheme.

3.1 Variational formulation

The variational formulation associated with Eqns. (12) - (15) over a typical two-node linear element $(y_e,\ y_{e+1})$ is given by:

$$
\int_{y_e}^{y_{e+1}} w_1 \left[\frac{\partial u}{\partial t} - A_1\left(\frac{\partial^2 u}{\partial y^2}\right) - (Gr\theta + Gm\phi) - A_2\left(\frac{\partial \omega}{\partial y}\right) \right] dy = 0 \tag{17}
$$

$$\int_{y_e}^{y_{e+1}} w_2\left[\frac{\partial \omega}{\partial t} - A_3\left(\frac{\partial^2 \omega}{\partial y^2}\right)\right]dy = 0 \tag{18}$$

$$\int_{y_e}^{y_{e+1}} w_3\left[\frac{\partial \theta}{\partial t} - A_4\left(\frac{\partial^2 \theta}{\partial y^2}\right) - Ec\left(\frac{\partial u}{\partial y}\right)^2\right]dy = 0 \tag{19}$$

$$\int_{y_e}^{y_{e+1}} w_4\left[\frac{\partial \phi}{\partial t} - \frac{1}{Sc}\left(\frac{\partial^2 \phi}{\partial y^2}\right) + \gamma\,\phi\right]dy = 0 \tag{20}$$

Here w_1, w_2, w_3 and w_4 are arbitrary test functions and may be viewed as the variations in u, ω , θ and ϕ respectively and $A_1 = 1+\beta$, $A_2 = \beta$, $A_3 = \left(\frac{1}{\eta}\right)$, $A_4 = \frac{1}{\Pr}(1+N)$. After dropping the order of integration and non-linearity, we arrive at the following system of equations.

$$\int_{y_e}^{y_{e+1}}\left[w_1\frac{\partial u}{\partial t} + A_1\frac{\partial w_1}{\partial y}\frac{\partial u}{\partial y} - (Gr\; w_1\theta + Gmw_1\phi) - A_2 w_1\frac{\partial \omega}{\partial y}\right]dy - \left[w_1\left(\frac{\partial u}{\partial y}\right)\right]_{y_e}^{y_{e+1}} = 0 \tag{21}$$

$$\int_{y_e}^{y_{e+1}}\left[w_2\frac{\partial \omega}{\partial t} - A_3\left(\frac{\partial w_2}{\partial y}\right)\left(\frac{\partial \omega}{\partial y}\right)\right]dy - \left[w_2\left(\frac{\partial \omega}{\partial y}\right)\right]_{y_e}^{y_{e+1}} = 0 \tag{22}$$

$$\int_{y_e}^{y_{e+1}}\left[w_3\frac{\partial \theta}{\partial t} - A_4\left(\frac{\partial w_3}{\partial y}\right)\left(\frac{\partial \theta}{\partial y}\right) - Ec\; w_3\left(\frac{\partial \bar{u}}{\partial y}\right)\left(\frac{\partial u}{\partial y}\right)\right]dy - \left[w_3\left(\frac{\partial \theta}{\partial y}\right)\right]_{y_e}^{y_{e+1}} = 0 \tag{23}$$

$$\int_{y_e}^{y_{e+1}}\left[w_4\frac{\partial \phi}{\partial t} + \frac{1}{Sc}\left(\frac{\partial w_4}{\partial y}\right)\left(\frac{\partial \phi}{\partial y}\right) + \gamma\,(w_4)\,\phi\right]dy - \left[\frac{w_4}{Sc}\left(\frac{\partial \phi}{\partial y}\right)\right]_{y_e}^{y_{e+1}} = 0 \tag{24}$$

3.2 Finite Element formulation

The finite element model may be obtained from Eqs. (21) - (24) by substituting *finite element approximations* of the form:

$$u = \sum_{j=1}^{2} u_j^e \psi_j^e,\; \omega = \sum_{j=1}^{2} \omega_j^e \psi_j^e,\; \theta = \sum_{j=1}^{2} \theta_j^e \psi_j^e \;and\; \phi = \sum_{j=1}^{2} \phi_j^e \psi_j^e \tag{25}$$

With $w_1 = w_2 = w_3 = w_4 = \psi_j^e$ $(i = 1, 2)$, where u_j^e, ω_j^e, θ_j^e *and* ϕ_j^e are the velocity in the direction of *x*-axis, *y*-axis and temperature respectively at the j^{th} node of typical e^{th} element (y_e, y_{e+1}) and ψ_i^e are the shape functions for this element (y_e, y_{e+1}) and are taken as:

$$\psi_1^e = \frac{y_{e+1} - y}{y_{e+1} - y_e} \text{ and } \psi_2^e = \frac{y - y_e}{y_{e+1} - y_e},\ y_e \le y \le y_{e+1} \tag{26}$$

The finite element model of the equations for the e^{th} element thus formed is given by.

$$\begin{bmatrix} [K^{11}] & [K^{12}] & [K^{13}] & [K^{14}] \\ [K^{21}] & [K^{22}] & [K^{23}] & [K^{24}] \\ [K^{31}] & [K^{32}] & [K^{33}] & [K^{34}] \\ [K^{41}] & [K^{42}] & [K^{43}] & [K^{44}] \end{bmatrix} \begin{bmatrix} \{U^e\} \\ \{\omega^e\} \\ \{\theta^e\} \\ \{\phi^e\} \end{bmatrix} + \begin{bmatrix} [M^{11}] & [M^{12}] & [M^{13}] & [M^{14}] \\ [M^{21}] & [M^{22}] & [M^{23}] & [M^{24}] \\ [M^{31}] & [M^{32}] & [M^{33}] & [M^{34}] \\ [M^{41}] & [M^{42}] & [M^{43}] & [M^{44}] \end{bmatrix} \begin{bmatrix} \{U'^e\} \\ \{\omega'^e\} \\ \{\theta'^e\} \\ \{\phi'^e\} \end{bmatrix} = \begin{bmatrix} \{b^{1e}\} \\ \{b^{2e}\} \\ \{b^{3e}\} \\ \{b^{4e}\} \end{bmatrix} \tag{27}$$

Where $\{[K^{mn}], [M^{mn}]\}$ and $\{\{u^e\}, \{\omega^e\}, \{\theta^e\}, \{\phi^e\}, \{u'^e\}, \{\omega'^e\}, \{\theta'^e\}, \{\phi'^e\} and \{b^{me}\}\}$ $(m, n = 1, \ ,2, 3, 4)$ are the set of matrices of order 2×2 and 2×1 respectively and *prime* $(')$ indicates $\frac{d}{dy}$. These matrices are defined as follows:

$$\begin{cases} K_{ij}^{11} = A_1 \int_{y_e}^{y_{e+1}} \left[\left(\frac{\partial \psi_i^e}{\partial y} \right) \left(\frac{\partial \psi_j^e}{\partial y} \right) \right] dy, K_{ij}^{12} = -A_2 \int_{y_e}^{y_{e+1}} \left[\left(\psi_i^e \right) \left(\frac{\partial \psi_j^e}{\partial y} \right) \right] dy, \\ K_{ij}^{13} = -Gr \int_{y_e}^{y_{e+1}} \left(\psi_i^e \right) \left(\psi_j^e \right) dy, K_{ij}^{14} = -Gm \int_{y_e}^{y_{e+1}} \left(\psi_i^e \right) \left(\psi_j^e \right) dy, \\ M_{ij}^{11} = \int_{z_e}^{z_{e+1}} \left(\psi_i^e \right) \left(\psi_j^e \right) dy, \quad M_{ij}^{12} = M_{ij}^{13} = M_{ij}^{14} = 0, \end{cases} \tag{28}$$

$$\begin{cases} K_{ij}^{21} = 0, K_{ij}^{22} = 0, K_{ij}^{23} = A_3 \int_{y_e}^{y_{e+1}} \left[\left(\frac{\partial \psi_i^e}{\partial y} \right) \left(\frac{\partial \psi_j^e}{\partial y} \right) \right] dy, \ K_{ij}^{24} = 0, \\ M_{ij}^{21} = M_{ij}^{22} = 0, M_{ij}^{23} = \int_{z_e}^{z_{e+1}} \left(\psi_i^e \right) \left(\psi_j^e \right) dy, \ M_{ij}^{24} = 0, \end{cases} \tag{29}$$

$$\begin{cases} K_{ij}^{31} = 0, K_{ij}^{32} = A_4 \int_{z_e}^{z_{e+1}} \left[\left(\frac{\partial \psi_i^e}{\partial y} \right) \left(\frac{\partial \psi_j^e}{\partial y} \right) \right] dy, K_{ij}^{33} = -Ec \int_{y_e}^{y_{e+1}} \left(\psi_i^e \right) \left(\frac{\partial \bar{u}}{\partial y} \right) \left(\frac{\partial \psi_j^e}{\partial y} \right) dy, K_{ij}^{34} = 0, \\ M_{ij}^{31} = 0, \ M_{ij}^{32} = 0, M_{ij}^{33} = \int_{y_e}^{y_{e+1}} \left(\psi_i^e \right) \left(\psi_j^e \right) dy, \quad M_{ij}^{34} = 0 \end{cases} \tag{30}$$

$$\begin{cases} K_{ij}^{41}=0, K_{ij}^{42}=0, K_{ij}^{43}=0, K_{ij}^{44}=\dfrac{1}{Sc}\displaystyle\int_{y_e}^{y_{e+1}}\left[\left(\frac{\partial \psi_i^e}{\partial y}\right)\left(\frac{\partial \psi_j^e}{\partial y}\right)\right]dy+\gamma\int_{y_e}^{y_{e+1}}\left(\psi_i^e\right)\left(\psi_j^e\right)dy, \\ M_{ij}^{41}=0, \quad M_{ij}^{42}=0, \quad M_{ij}^{43}=\displaystyle\int_{y_e}^{y_{e+1}}\left(\psi_i^e\right)\left(\psi_j^e\right)dy, \quad M_{ij}^{44}=0 \end{cases} \tag{31}$$

$$\begin{cases} b_i^{1e}=\left[\left(\psi_i^e\right)\left(\dfrac{\partial u}{\partial y}\right)\right]_{y_e}^{y_{e+1}}, \; b_i^{2e}=\left[\left(\psi_i^e\right)\left(\dfrac{\partial \omega}{\partial y}\right)\right]_{y_e}^{y_{e+1}}, \\ b_i^{3e}=\left[\left(\psi_i^e\right)\left(\dfrac{\partial \theta}{\partial y}\right)\right]_{y_e}^{y_{e+1}}, b_i^{4e}=\left[\left(\psi_i^e\right)\left(\dfrac{\partial \phi}{\partial y}\right)\right]_{y_e}^{y_{e+1}} \end{cases} \tag{32}$$

In one dimensional space, linear and quadratic elements or higher order can be taken. Here the entire flow domain is considered by dividing it into successively sized grids of order 81x81, 101x101 and 121x121 in the y-axis direction. After many tests a grid size with 101 intervals has been adopted. Thus all the computations are executed with 101 intervals of equal step size 0.01. At each node, 4 functions are to be evaluated and after assembly of the element equations, a set of 404 non-linear equations are obtained which necessitate an iterative solution subject to the specified boundary conditions. The iterative process is terminated when the following condition is met: $\sum_{i,j}\left|\xi^{n+1}-\xi^{n}\right|\le 10^{-6}$ where $\xi=U,\omega,\theta,\phi$ and n denote the iterative step. In order to see the effects of step size (h) the finite element code is run with step sizes as h=0.01 and very good agreement is obtained for different profiles. Hence, this method has been proven to be adequate and gives accurate results for the conservation equations. It is also important to compute engineering quantities of primary interest, which are the skin-friction, wall couple stress (surface micro-rotation gradient), Nusselt number and Sherwood number.

Skin-friction is obtained as,

$$C_f=\left[\frac{\partial u}{\partial y}\right]_{y=0} \tag{33}$$

Wall couple stress is defined as,

$$C_m=\left[\frac{\partial \omega}{\partial y}\right]_{y=0} \tag{34}$$

The *Nusselt number* is computed as,

$$Nu / \mathrm{Re}_x = -\left[\frac{\partial \theta}{\partial y}\right]_{y=0} \tag{35}$$

The *Sherwood number* is evaluated as,

$$Sh / \mathrm{Re}_x = -\left[\frac{\partial \phi}{\partial y}\right]_{y=0} \tag{36}$$

3.3 Study of Grid Independence

In general, to study the grid independency (or) dependency, we check how the mesh size should be varied at different mesh (grid) sizes and get a range at which there is no subsequent variation in the solutions. For this purpose, we have presented numerical values of velocity, temperature and concentration for different values of mesh sizes at time $t = 0.2$ in the **Table 1**, which shows that no variations in velocity, angular velocity, temperature and concentration. Hence the results are independent of mesh size.

4. VALIDATION OF NUMERICAL RESULTS

To verify the accuracy and validity of the numerical results employed by the weighted residual approach and the Galerkin finite element method, the results have been compared to the analytical solutions for local skin friction coefficient and wall couple stress coefficient reported by Khalid *et al.* [14] for different values of $\beta, n, \mathrm{Pr}, Gr, Gm, Sc, \alpha t,$ and t in **Table 2.** These solutions negate thermal radiation, viscous dissipation and homogeneous chemical reaction effects, since these terms were ignored in the model of Khalid *et al.* [14]. Generally, very good correlation is achieved. **Table 2** further shows that in the absence of radiative flux, chemical reaction or viscous heating, skin friction increases as $\beta, \mathrm{Pr}, Sc, \alpha t$ increase but decreases with a rise in n, Gr, Gm, t. Further, it is observed that wall couple stress decreases as $\beta, n, \mathrm{Pr}, Gr, Gm, Sc, \alpha t,$ and t increase.

5. GRAPHICAL RESULTS AND DISCUSSION

In order to gain a clear insight into the physical problem, numerical calculations for distribution of the velocity, microrotation (angular) velocity, temperature and concentration for different values of the control parameters are illustrated in **Figs. (2) - (27**). In order to study the effects of

pertinent parameters in fluid flow explicit computations were carried out by varying micro-rotation parameter β, dimensionless spin gradient viscosity parameter η, microelement surface condition n, Grashof number Gr, species Grashof number Gm, Prandtl number Pr, radiative-conduction parameter N, Eckert number Ec, Schmidt number Sc, phase angle ωt and chemical reaction parameter γ.

Figures 2-3 illustrate the influence of micro-rotation parameter β on velocity and micro-rotation profiles. It is evident that velocity distribution is greater for a Newtonian fluid (β=0) with the given parameters, as compared with non-Newtonian fluid (micropolar fluid). Peak values are attained close to the plate and these migrate away from the plate with increasing β. All profiles decay from the peak to vanish in the free stream velocity. In addition, the micro-rotation (fig. 3) i.e. angular velocity takes negative values throughout the regime. The lowest values are at the plate surface and approach zero as one moves away from the plate surface which agrees with the imposed boundary condition on micro-rotation. Hence micro-rotation velocity profiles increase as β increases.

Figures 4, 5 present the velocity and angular velocity (micro-rotation) profiles for various values of spin gradient viscosity parameter η. It is observed from that velocity increases as spin gradient viscosity parameter η increases whereas micro-rotation is strongly reduced i.e. the gyratory motion of the micro-elements is decelerated with greater spin gradient viscosity. Drag in the linear velocity field is however reduced and significant acceleration induced with greater spin gradient viscosity and indeed this concurs with many other studies in micropolar fluid mechanics including Hossain and Chowdhury [60].

Figures 6 and 7 depict the effect of microelement surface condition (n) on both velocity and micro-rotation profiles. Micro element parameter n, describes the relation between micro-gyration vector and shear stress. It is observed that the velocity increases with increasing values of n. Furthermore the momentum boundary layer thickness is decreased with greater n values, and this is attributable to the smaller micro-gyration vector. The impact of increasing n however diminishes with greater distance from the plate. Micro-rotation velocity increases as n increases, although values are always negative. All profiles converge smoothly to zero in the free stream i.e. the influence of n strongly decreases with progressive distance from the plate.

Figures 8 and 9 shows the variations in velocity and microrotation velocity profiles for various values of thermal Grashof number, Gr. Gr quantifies the relative magnitude of the buoyancy force and the opposing frictional (viscous) forces acting on the micropolar fluid. Physically the positive, negative and zero $(i.e.,\ Gr > 0, Gr < 0\ and\ Gr = 0)$ values of the Grashof number represents the cooling, heating of the boundary surface and absence of free convection currents respectively. The velocity profiles are significantly elevated with an increase in thermal Grashof number, since buoyancy assists in momentum development. The flow is therefore strongly accelerated for the case where the plate is cooled (Gr >0). Velocity profiles exhibit a parabolic distribution, ascending from the plate, achieving a peak value near the plate and then decaying to vanish in the free stream, far from the plate. Conversely an increase in thermal Grashof number strongly damps the micro-rotation field i.e. decreases angular velocity of the micro-elements. Again values are consistently negative indicating a reverse spin in the micro-elements. As with linear velocity, in the free stream micro-rotation vanishes and is generally minimized at the plate.

Figures 10, 11 present the response in linear velocity and micro-rotation to a variation in species (solutal) Grashof number i.e. Gm. This parameter embodies the relative contribution of species buoyancy force to viscous hydrodynamic force. With increasing *Gm*, the mass diffusion effect leads to an acceleration in the flow i.e. increase in velocity values and an associated decrease in hydrodynamic boundary layer thickness. We note that for the case $Gm = 0$, species buoyancy effect vanishes and the momentum eqn. (12) is *de-coupled* from the species diffusion (concentration) eqn. (15). Micro-rotation values are significantly reduced with increasing *Gm* values i.e. increasing species buoyancy (associated with greater concentration gradient) exerts a similar influence to increasing thermal buoyancy and strongly damps the angular velocity. The spin of the micro-elements is therefore markedly inhibited with greater buoyancy effects.

Figures 12-13 illustrate the evolution in linear velocity and micro-rotation distributions with different values of phase angle ωt. A weak oscillatory behavior is computed for the linear velocity and with increasing phase angle (three different values are chosen) there is a progressive deceleration in the flow. Infact at maximum phase angle, flow reversal is induced since the linear velocities attain negative values at $\omega t = \pi$. At zero phase angle the maximum velocity is achieved at the plate whereas for $\omega t = \pi$, the maximum velocity is attained in the free stream.

Strong damping is therefore generated in the flow with increasing phase angle. Conversely an increase in phase angle is observed to enhance the micro-rotation i.e. it increases angular velocity. Greater oscillation of the plate encourages spin of the micro-elements and in all cases the minimum micro-rotations (maximum negative values) arise at the plate eventually vanishing in the free stream.

Figures 14-16 illustrate the influence of Prandtl number (*Pr*) on the linear, angular velocity (micro-rotation) and temperature profiles. With greater Prandtl number, it is observed in fig. 14, that the velocity is significantly decreased throughout the boundary layer. Prandtl number represents the relative rate of momentum diffusion to energy diffusion. For $Pr < 1$ energy diffusion rate exceeds momentum diffusion. Also fluids with higher Prandtl number possess greater viscosities and as *Pr* increases from 0.3 through 0.5, 0.7 to 0.9, the viscous resistance leads to depletion in velocity. This will also manifest in an increase in momentum (hydrodynamic) boundary layer thickness. Similarly there is a strong depression in micro-rotation (fig. 15) with increasing Prandtl number. The coupling of the linear and angular momentum equations manifests in an indirect deceleration in the micro-element gyratory motions (micro-rotation) due to damping of the linear velocity field. Temperature is also significantly suppressed with greater Prandtl number, as plotted in fig. 16. Greater Prandtl number corresponds to a lower thermal conductivity. This leads to a reduction in thermal energy convected through the fluid from the plate ($Gr > 0$ i.e. plate cooling) and also depresses the thermal boundary layer thickness. These trends have also been computed by numerous other researchers including Rahman and Sultana [7].

Figures 17-19 present the effect of thermal radiation-conduction parameter (N) on respectively linear velocity, micro-rotation and temperature profiles. This parameter is defined as $N = \frac{16\bar{\sigma} T_{\infty}^3}{3k \bar{k}}$ and features in the augmented thermal diffusion term in eqn. (14) i.e. $\frac{1}{\Pr}(1+N)\frac{\partial^2 \theta}{\partial y^2}$.

It defines the relative contribution of thermal radiation heat transfer to thermal conduction heat transfer. When $N < 1$ thermal conduction dominates. When $N = 1$ both thermal conduction and thermal radiation contributions are equal. For $N > 1$ thermal radiation dominates over thermal conduction. In the present simulations, we confine attention to the last of these three cases. Fig. 17 clearly reveals that there is a strong deceleration in the linear velocity with increasing *N*

values. The energizing of the flow enhances thermal diffusion but counteracts momentum diffusion. This leads to an increase in momentum boundary layer thickness. A similar observation has been reported by Abo-Eldahab and Ghonaim [28] and Olajuwon and Oahimire [29]. Conversely increasing *N* values are found to elevate the micro-rotation of micro-elements as observed in fig. 18. Increasing radiation-conduction parameter is also found to decrease temperatures in the boundary layer (fig. 19). Thermal boundary layer thickness is therefore also reduced with greater values of *N*.

Figures 20-22 present the effects of the viscous dissipation parameter i.e., the Eckert number Ec on the velocity, micro-rotation and temperature fields. Eckert number signifies the quantity of mechanical energy converted via internal friction to thermal energy i.e. heat dissipation. Increasing *Ec* values will therefore cause an increase in thermal energy contributing to the flow and will heat the regime. Positive Eckert number implies cooling of the wall and therefore a transfer of heat to the micropolar fluid. Convection is enhanced and we observe in consistency with this that at the fluid is accelerated i.e. linear velocity is elevated (fig. 20). Similarly there is an enhancement in micro-rotation in the micropolar fluid with increasing *Ec* values (fig. 21). Temperatures are markedly increased with greater Eckert number (fig. 22). For all non-zero values of *Ec the* temperature overshoot near the wall is distinct, this overshoot migrates marginally further into the boundary layer with an increase in *Ec*. Very smooth decays in temperature profiles are observed for all values of Eckert number and the convergence of profiles in the free stream indicates that an adequately large infinity boundary condition has been imposed in the finite element model.

Figures 23-25 illustrate the velocity, micro-rotation and concentration profiles for different values of Schmidt number, *Sc*. The Schmidt number embodies the ratio of the momentum to the mass diffusivity i.e. $Sc = \nu / D$. The Schmidt number therefore quantifies the relative effectiveness of momentum and mass transport by diffusion in the hydrodynamic (velocity) and concentration (species) boundary layers. For $Sc > 1$ momentum diffusion rate *exceeds* the species diffusion rate. The opposite applies for *Sc < 1*. For *Sc =1* both momentum and concentration (species) boundary layers will have the same thickness and diffusivity rates will be equal. It is observed that as the Schmidt number increases velocity, angular velocity and concentration all decrease. The momentum boundary layer thickness is also reduced with greater Schmidt number. The suppression in micro-rotation is associated with a deceleration in the linear

velocity field. The depression in concentration magnitudes is due to the reduction in molecular diffusivity which manifests in a stifled migration of species. Concentration boundary layer thickness is therefore also decreased with increasing Schmidt number.

Figures 26-27 represents the influence of chemical reaction parameter (γ) on the velocity and concentration profiles. The reaction parameter is based on a first-order irreversible chemical reaction which takes place both in the bulk of the fluid (homogeneous) as well as at plate which is assumed to be catalytic to chemical reaction. Although chemical reactions generally fall into one of two categories i.e. homogenous or heterogenous, the former is of interest in the present study. Homogenous chemical reactions take place uniformly throughout a given phase and are similar in nature to an internal source of heat generation. We consider the destructive type of homogenous chemical reaction. Increasing the chemical reaction parameter γ produces a decrease in velocity (fig. 26). The momentum boundary layer thickness is therefore increased substantially with greater chemical reaction effect. It is noticed that concentration distributions decrease when the chemical reaction increases. Physically, for a destructive case, chemical reaction takes place and progressively destroys the original species. This, in turn, suppresses molecular diffusion of the remaining species which leads to a fall in concentration magnitudes and a decrease in concentration boundary layer thickness.

Finally **fig. 28** illustrates the difference in linear velocity for Newtonian and micropolar fluids. Strong deceleration is present for the micropolar case. The presence of micro-elements therefore achieves lower acceleration compared with Newtonian fluids which ignore microstructural effects.

6. CONCLUSIONS

In this work motivated by applications in materials processing of slurry systems, a mathematical model has been developed for conjugate free convection heat and mass in transient flow of an incompressible, micropolar fluid from an oscillating vertical plate in porous media. Viscous heating, thermal radiation and homogeneous chemical reaction effects have been incorporated into the model. The conservation equations for momentum, angular momentum (micro-rotation component), energy and concentration have been non-dimensionlized with appropriate variables. The resulting non-linear, transient, coupled system of partial differential equations and set of

initial and boundary conditions has been solved numerically, using the variational finite element method with Galerkin weighted residual scheme. Validation for solution for selected cases has been conducted with previous published works i.e. Khalid *et al.* [14] and excellent correlation achieved. A grid independence study has also been performed. The computations have been executed in MATLAB software, and have shown that:

- The flow is accelerated and momentum boundary layer thickness decreased with increasing values of η, n, Gr, Gm, and Ec.
- The flow is decelerated and momentum boundary layer thickness increased with increasing values of β, $\Pr$, αt, N, Sc and γ.
- Angular velocity (micro-rotation) is suppressed and micro-rotation boundary layer thickness increased with increasing of η, n, Gr, Gm, $\Pr$ and Sc. Conversely angular velocity is elevated with increasing values of β, αt, N and Ec.
- Increasing radiation-conduction parameter and Prandtl number decrease temperatures and thermal boundary layer thickness.
- Increasing Eckert number elevates temperatures and enhances thickness of thermal boundary layer.
- Increasing Schmidt number decreases velocity, micro-rotation and also concentration values and furthermore increases momentum boundary layer thickness but reduces concentration boundary layer thickness.
- Increasing homogeneous chemical reaction parameter decreases velocity and concentrations i.e. increases momentum boundary layer thickness and reduces concentration boundary layer thickness.
- The velocity magnitudes are lower for micropolar fluid compared with Newtonian fluids.

The present study has shown that the finite element method is very versatile in simulating *unsteady micropolar materials processing transport phenomena*. However a relatively simple radiative heat flux model has been used and also reaction effects restricted to first order. Future studies will consider more complex radiative models [61] and also higher order chemical reaction and will be communicated soon.

ACKNOWLEDGEMENTS

This research did not receive any specific grant from funding agencies in the public, commercial, or not- for profit sectors.

REFERENCES

[1] Eringen, A.C, Theory of micropolar fluids, *Journal of Applied Mathematics and Mechanics*, 16, 1-18 (1966).

[2] Eringen, A.C, Theory of thermo micropolar fluids, *Journal of Mathematical Analysis and Applications, 38*, 480-496 (1972).

[3] Eringen, A.C, *Micro-continuum field theories II Fluent media*, *Springer*, New York (2001).

[4] Lukaszewicz, G, *Micropolar Fluids, Modelling and Simulation*, Birkhauser Boston, Boston, (1999).

[5] Airman, T, Turk, M.A, Sylvester, N.D, Applications of micro-continuum fluid mechanics-a review, *Int. J. Eng. Sci.* 12, 273-293 (1974).

[6] Gupta, D., L. Kumar, O. Anwar Bég and Bani Singh, Finite element simulation of mixed convection flow of micropolar fluid over a shrinking sheet with thermal radiation, *Proc IMechE-Part E: J. Process Mechanical Engineering,* 228 (1) 61-72 (2014).

[7] Rahman, M.M, Sultana, Y, Radiative heat transfer flow of micropolar fluid with variable heat flux in porous medium, *Nonlinear Analysis, Modelling and Control*, *13*, 71-87 (2008).

[8] Reddy, M. G., Magnetohydrodynamics and radiation effects on unsteady convection flow of micropolar fluid past a vertical porous plate with variable wall heat flux, *ISRN Thermodynamics*, 4, 1-8 (2012).

[9] J. Zueco, O. Anwar Bég, H.S. Takhar, Network numerical analysis of magneto-micropolar convection through a vertical circular non-Darcian porous medium conduit, *Computational Materials Science*, 46, 4, 1028-1037 (2009).

[10] Aziz, A, A similarity solution for laminar thermal boundary layer over a flat plate with a convective surface boundary condition. *Commun. Nonlinear Sci. Numer. Simul.* 14, 1064–1068 (2009).

[11] Pop, I, Merkin J.H, Conjugate free convection on a vertical surface in a saturated porous medium, *Fluid Dynamic Research*, 16, 71-86 (1995).

[12] Merkin, J. H, Pop, I, Conjugate free convection on a vertical surface. *Int. J. Heat Mass Transfer,* 39, 1527-1534 (1996).

[13] Char, M.I, Chen, C.K, Cleaver, J.W, Conjugate forced convection heat transfer from a continuous moving flat sheet, *Int. J. Heat and Fluid Flow*, 11(3) 257-261 (1990).

[14] Khalid, A, I. Khan, Arshad Khan, Sharidan shafie, Conjugate transfer of heat and mass in unsteady flow of a micropolar fluid with wall couple stress, *AIP Advances*, 5, 127125 (2015).

[15] Chaudhary, R.C, Jain, A, Combined heat and mass transfer effects on MHD free convective flow past an oscillating plate embedded in porous medium, *Romanian Journal of Physics*, 52, 505-524 (2007).

[16] Hussain, A, Anwar, M.I, Ali, F, Khan, I, Natural convection flow past an oscillating plate with newtonian heating, *Heat Transfer Research*, 45, 119-137 (2014).

[17] Zhang, L, *Conjugate Heat and Mass Transfer in Heat Mass Exchanger Ducts*, Ist ed. Oxford, Elsevier (2013).

[18] Bejan, A. *Convection Heat Transfer*. 2nd ed. NY: Wiley (1993).

[19] Arpaci, V.S, Effect of thermal radiation on the laminar free convection from a heated vertical plate, *Int. J. Heat Mass Transfer,* 11, 871–881 (1968).

[20] England, W. G, Emery, A.F, Thermal radiation effects on the laminar free convection boundary layer of an absorbing gas, *ASME J. Heat Transfer* 91, 37–44 (1969).

[21] Özisik, M.N, *Thermal Radiation Transfer and Interactions with Conduction and Convection* Wiley, New York (1973).

[22] Bestman, A.R, Adjepong, S.K, Unsteady hydromagnetic free-convection flow with radiative heat transfer in a rotating fluid. *Astrophysics. Space Sci.* 143, 217–224 (1988).

[23] Molla, M.M, Hossain, M.A, Radiation effect on mixed convection laminar flow along a vertical wavy surface, *Int. J. Thermal Sci,* 46, 926-935 (2007).

[24] Jang, J.H, Chiu, H.C, Yan, W.M, Combined mixed convection and radiation heat in rectangular ducts rotating about a parallel axis, *Int. J. Heat Mass Transfer,* 50, 4229–4242 (2007).

[25] Jang, J.H, Chiu, H.C, Yan, W.M, Mixed convection heat transfer in horizontal rectangular ducts with radiation effects, *Int. J. Heat Mass Transfer*, 50, 2874–2882 (2007).

[26] Siddiqa, S, Asghar, S, Hossain, M.A, Radiation effects on natural convection flow over an inclined flat plate with temperature-dependent viscosity. *Proc. Inst. Mech. Eng. Part C*: *J. Mech. Eng. Sci.,* 225, 407–419 (2011).

[27] Siddiqa, S, Hossain, M.A, Mixed convection boundary layer flow over a vertical flat plate with radiative heat transfer, *Appl. Math.,* 3, 400–415 (2012).

[28] Abo-Eldahab, E.M, Ghonaim, A.F, Radiation effect on heat transfer of a micropolar fluid through a porous medium, *App. Math. Comput,* 169 (1), 500-516 (2005).

[29] Olajuwon, B.I, Oahimire, J.I, Unsteady free convection heat and mass transfer in an MHD micropolar fluid in the presence of thermo diffusion and thermal radiation, *Int. J. Pure and Applied Mathematics,* vol.84: 015-037 (2013).

[30] Kundu, P.K, Das, K, Jana, S, MHD micropolar fluid flow with thermal radiation and thermal diffusion in a rotating frame, *Bull. Malays. Math. Sci. Soc.*, Vol.38: 1185-1205 (2015).

[31] R. C. Warren, Viscous heating, Chapter 7, *Rheological Measurement, A. Collyer et al. (Eds),* Chapman and Hall, pp 210-236 (1998).

[32] C-H. Chen, Combined heat and mass transfer in MHD free convection from a vertical surface with Ohmic heating and viscous dissipation, *Int. J. Eng. Sci.* 42, 699-713 (2004).

[33] Reddy, M.G, Reddy, N.B, Radiation and mass transfer effects on unsteady MHD free convection flow past a vertical porous plate with viscous dissipation, *Int. J. Appl. Math. Mech,* 6 (6), 96–110 (2010).

[34] Srinivasacharya, D, Upender, M, Thermal radiation and chemical reaction effects on MHD free convection heat and mass transfer in a micropolar fluid, *Turk. J. Eng. Environmental. Sci.* 38 (2015) 184-196.

[35] Siva Reddy, S, Shamshuddin, MD, Heat and mass transfer on the MHD flow of a micropolar fluid in the presence of viscous dissipation and chemical reaction, *Procedia Eng.,* 127, 885-892 (2015).

[36] Siva Reddy, S., Shamshuddin, MD, Diffusion-thermo and chemical reaction effects on an unsteady MHD free convection flow in a micropolar fluid. *Theoretical and Applied Mechanics,* 43, 117-131 (2016).

[37] Rawat, S., S. Kapoor, R. Bhargava and O. Anwar Bég, Heat and mass transfer of a chemically-reacting micropolar fluid over a linear stretching sheet in a Darcy-Forchheimer porous medium, *Int.J. Computer Applications,* 44, 40-51, (2012).

[38] Pal, D., Talukdar, B., Perturbation technique for unsteady MHD mixed convection periodic flow, heat and mass transfer in micropolar fluid with chemical reaction in the presence of thermal radiation, *Central European J. Physics*, 10, 1150-1167 (2012).

[39] Reis, N. M. F. Novel oscillatory flow reactors for biotechnological applications. *PhD Thesis, School of Engineering, University of Minho, Portugal* (2006).

[40] B. Pan and B.Q. Li, Effect of magnetic fields on oscillating mixed convection, *International Journal of Heat and Mass Transfer*, 41, 2705-2710 (1998).

[41] S. O. Adesanya, J. A. Falade and O.D. Makinde, MHD oscillatory slip flow and heat transfer in a channel filled with porous media, *U.P.B Scientific Bulletin A*, 76, pp197- 204 (2014).

[42] R Bhargava, R Sharma, OA Bég, Oscillatory chemically-reacting MHD free convection heat and mass transfer in a porous medium with Soret and Dufour effects: finite element modeling, *Int. J. Appl. Math. Mech* 5 (6), 15-37(2012).

[43] S. O. Adesanya, Free convective flow of heat generating fluid through a porous vertical channel with velocity slip and temperature jump, *Ain Shams Engineering Journal*, 6, 1045–1052 (2014).

[44] V. Rajesh, O. Anwar Bég and C. Sridevi, Finite difference analysis of unsteady MHD free convective flow over moving semi-infinite vertical cylinder with chemical reaction and temperature oscillation effects, *J. Appl. Fluid Mech.* 9, 157-167 (2016).

[45] S. O. Adesanya, J. A. Falade and O.D. Makinde, Pulsating flow through vertical porous channel with viscous dissipation effect, *U.P.B. Sci. Bull., Series D - Mechanical Engineering*, 77, 25-36 (2015).

[46] K. Maqbool, Ayesha Sohail, Shafaq Idreesa and O. Anwar Bég, Analytical solutions for magnetohydrodynamic oscillatory rotating plate and channel flows in porous media using a fractional Burgers viscoelastic model, *European Physical Journal Plus, 131: 140-157 (2016).*

[47] S. O. Adesanya, E.O.Oluwadare, J. A. Falade and O.D. Makinde Hydromagnetic natural convection flow between vertical parallel plates with time-periodic boundary conditions, *Journal of Magnetism and Magnetic Materials*, 396, 295–303 (2015).

[48] O. Anwar Bég, S.K. Ghosh and M. Narahari, Mathematical modelling of oscillatory MHD Couette flow in a rotating highly permeable medium permeated by an oblique magnetic field, *Chemical Engineering Communications, 198, 235-254 (2010).*

[49] Srinivasacharya, D, Upendar, M, Free convection in MHD micropolar fluid with radiation and chemical reaction effects, *Chem. Ind. Chem. Eng. Q.* 20 (2), 183-195 (2014).

[50] Magyari, E, Pantokratoras, A, Note on the effect of thermal radiation in the linearized Rosseland approximation on the heat transfer characteristics of various boundary layer flows, *Int. Commun. Heat Mass Transfer*, 38, 554–556 (2011).

[51] Rapits A, Perdikis, C, Viscoelastic flow by the presence of radiation. *ZAMP*, 78, 277–279 (1998).

[52] Cortell, R, A numerical tackling on Sakiadis flow with thermal radiation. *Chin Physics Let:* 25: 1340–1342 (2008).

[53] Hayat T, Mustafa M, Sajid, M, Influence of thermal radiation on Blasius flow of a second grade fluid. *Z Naturforsch* 64a: 827–833 (2009).

[54] Reddy, J.N, *An Introduction to the Finite Element Method*, *McGraw-Hill*, New York (1985).

[55] Bathe, K.J.: *Finite Element Procedures*, *Prentice-Hall*, New Jersey, USA (1996).

[56] O. Anwar Bég, M.M. Rashidi, and R. Bhargava, *Numerical Simulation in Micropolar Fluid Dynamics*, Lambert: Sarbrucken, Germany, 288pp (2011).

[57] O. Anwar Bég, R. Bhargava, S. Rawat, H. S. Takhar and T. A. Bég, A study of buoyancy-driven dissipative micropolar free convection heat and mass transfer in a Darcian porous medium with chemical reaction, *Nonlinear Analysis: Modeling and Control*, 12, 2, 157-180 (2007).

[58] O. Anwar Bég, R. Bhargava, S. Rawat, H. S. Takhar, M. Kalim Halim, Computational modeling of biomagnetic micropolar blood flow and heat transfer in a two-dimensional non-Darcian porous medium, *Meccanica J.*, 43, 391-410 (2008).

[59] R. Bhargava, S. Sharma, P. Bhargava, O. Anwar Bég and A. Kadir, Finite element simulation of nonlinear convective heat and mass transfer in a micropolar fluid-filled enclosure with Rayleigh number effects, *Int. J. Applied Computational Mathematics*, 3, 1347-1379 (2017).

[60] M.A. Hossain and M. K. Chowdhury, Mixed convection flow of micropolar fluid over an isothermal plate with variable spin gradient viscosity, *Acta Mechanica*, 131, 139-151 (1998).

[61] O. Anwar Bég, N. Ali, A. Zaman, Eemaan T. A. Bég and Ayesha Sohail, Computational modelling of heat transfer in annular porous medium solar energy absorber with a P1-radiative differential approximation, *J. Taiwan Inst. Chemical Eng.*, 66, 258-268 (2016).

Nomenclature

C Concentration of the solute [$mol\ m^{-3}$]

C_f Skin friction coefficient

C_m Wall couple stress

C_p Specific heat at constant pressure [$J\ Kg^{-1}K^{-1}$]

C_w Concentration of the solute at the plate [$mol\ m^{-3}$]

C_∞ Free stream concentration [$mol\ m^{-3}$]

D_m Molecular diffusivity [$m^2 s^{-1}$]

Ec Eckert number

g^* Acceleration due to gravity [ms^{-1}]

G_m Solutal Grashof number

G_r Grashof number

H Unit step function

$\vec{i}$ Unit vector in flow direction

J' Micro inertia coefficient

n micro-element surface condition

N Radiative-conduction parameter

Nu Nusselt number

p constant pressure

P_r Prandtl number

q_r Radiative heat flux [$W\ m^{-2}$]

Re_x Local Reynolds number

Sc Schmidt number

Sh_x Sherwood number

t dimensionless time

T Temperature of the field in the boundary layer [K]

T_w wall temperature of the fluid [K]

T_∞ Temperature of the fluid in free stream [K]

U Amplitude of the motion

V Plate velocity

x' Axis along the plate [m]

y' Axis perpendicular to the plate [m]

w_1, w_2, w_3, w_4 Arbitrary test functions

Greek letters

α Frequency oscillations

β Viscosity ratio parameter

β_c Volumetric coefficient of concentration expansion[K^{-1}]

β_f Volumetric coefficient of concentration expansion [K^{-1}]

η Dimensionless spin gradient viscosity ratio parameter

αt Phase angle

ρ Density of micropolar fluid [$kg\ m^{-3}$]

κ Thermal conductivity [$Wm^{-1}K^{-1}$]

$\overline{\kappa}$ Mean absorption coefficient [m^{-1}]

$\overline{\sigma}$ Stefan-Boltzmann constant [$Wm^{-2}K^{-4}$]

ν Kinematic viscosity [$m^2 s^{-1}$]

Λ Coefficient of gryo-viscosity

μ Fluid dynamic viscosity

γ_o Spin gradient viscosity

γ Dimensionless chemical reaction parameter

θ Dimensionless temperature

ϕ Dimensionless concentration

ψ Shape function

ω Microrotation component

Figures

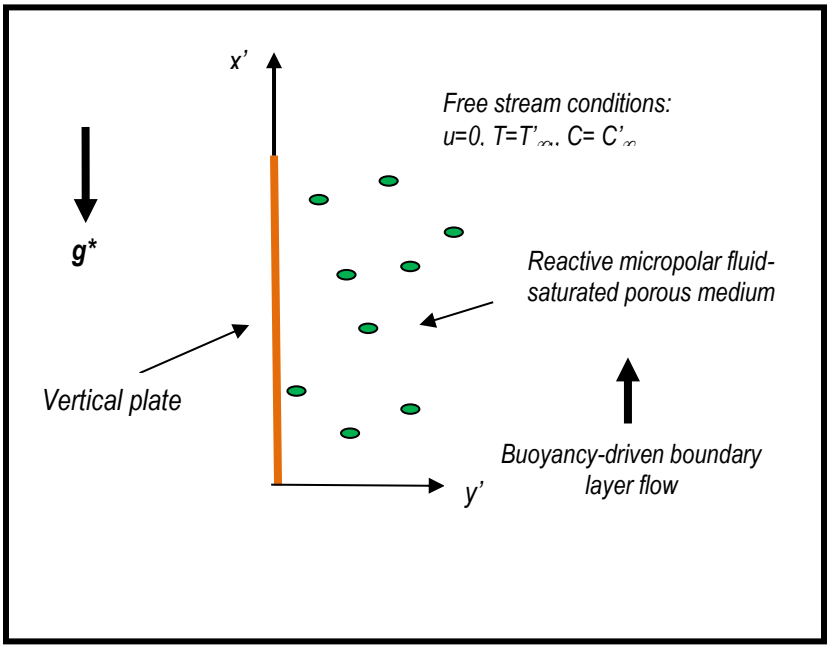

Figure 1: Flow configuration and coordinate system

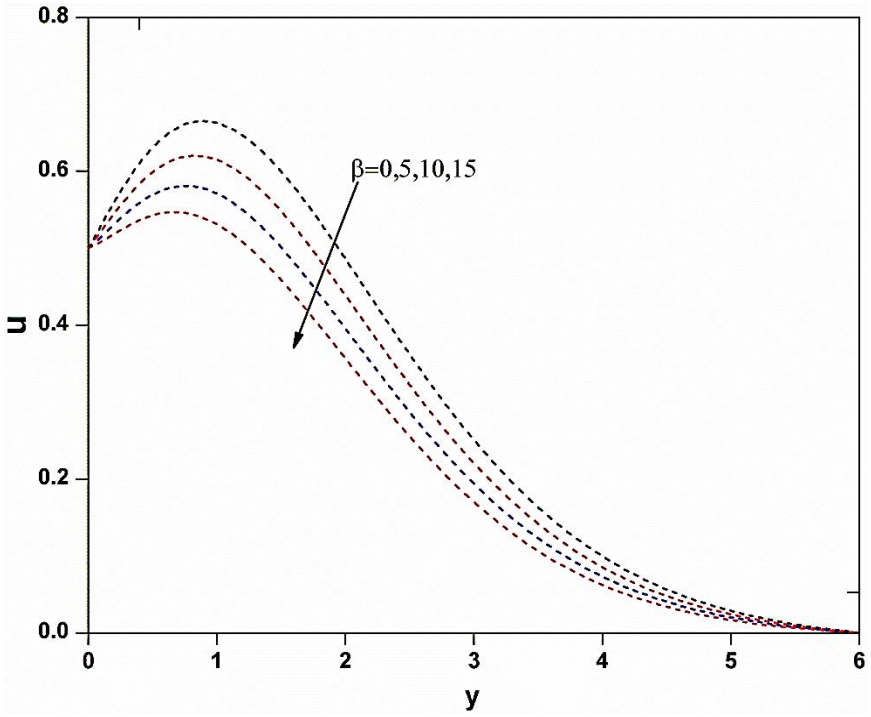

Figure 2: Velocity profiles for various values of β , when $t = 0.2, \eta = 1.5, n = 0.6, \alpha t = \pi / 3$ $Gr = 5, Gm = 10, \Pr = 0.3, N = 3, Ec = 0.01, Sc = 0.2, \gamma = 1$.

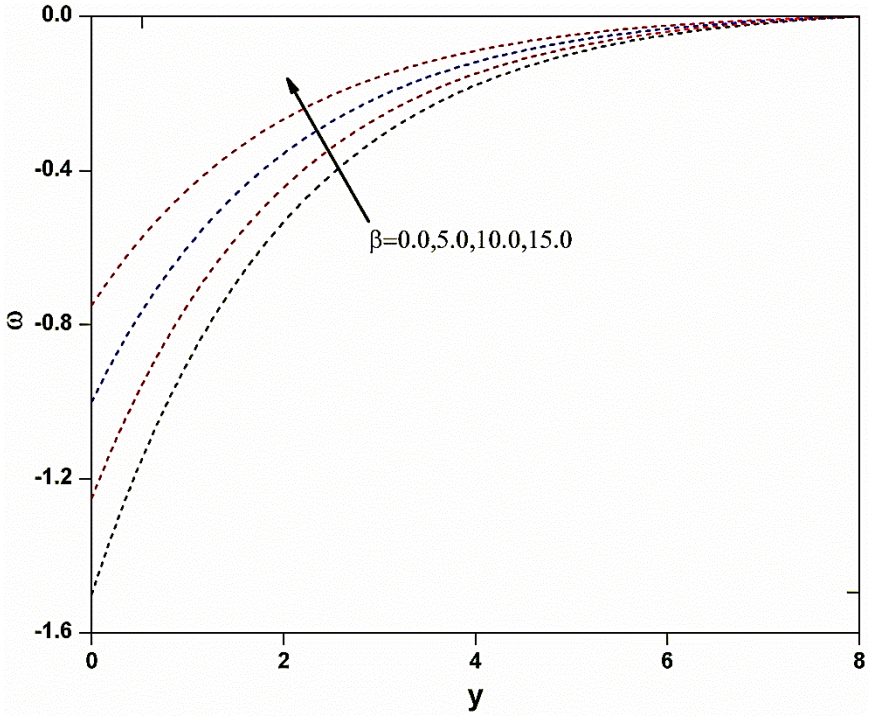

Figure 3: Micro-rotation profiles for various values of β , when $t = 0.2, \eta = 1.5, n = 0.6, \alpha t = \pi / 3$ $Gr = 5, Gm = 10, \Pr = 0.3, N = 3, Ec = 0.01, Sc = 0.2, \gamma = 1$.

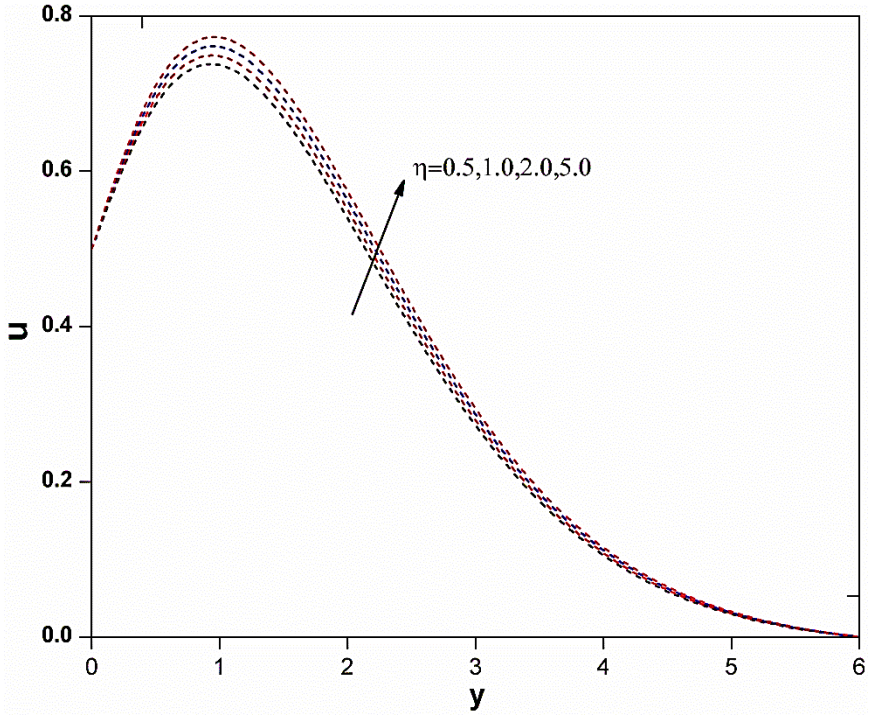

Figure 4: Velocity profiles for various values of η , when $t = 0.2, \beta = 0.5, n = 0.6, \alpha t = \pi / 3,$ $Gr = 5, Gm = 10, \Pr = 0.3, N = 3, Ec = 0.01, Sc = 0.2, \gamma = 1$.

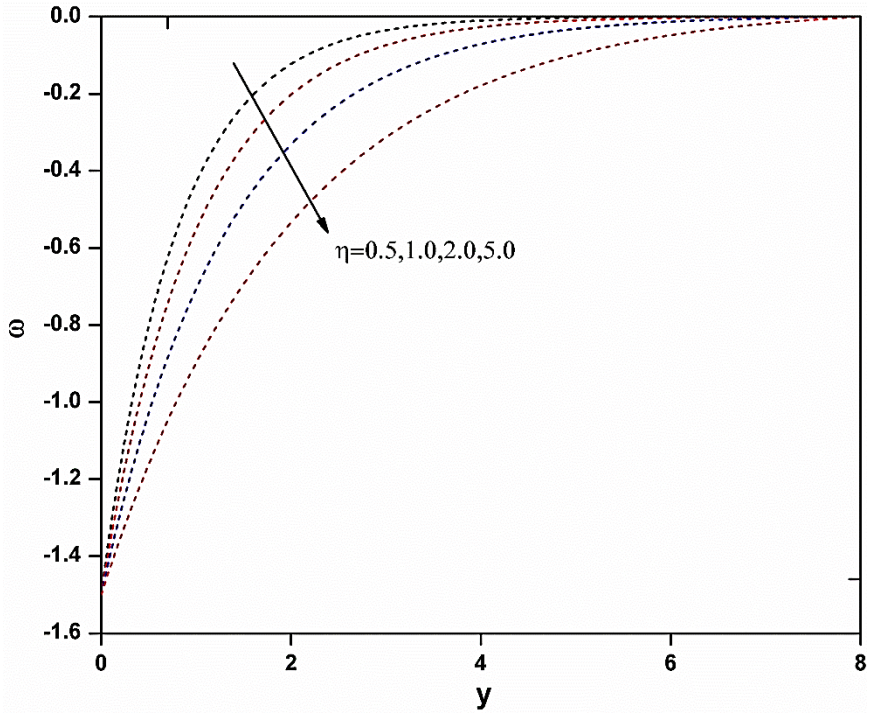

Figure 5: Micro-rotation profiles for various values of η, when $t = 0.2, \beta = 0.5, n = 0.6, \alpha t = \pi/3$ $Gr = 5, Gm = 10, \Pr = 0.3, N = 3, Ec = 0.01, Sc = 0.2, \gamma = 1$.

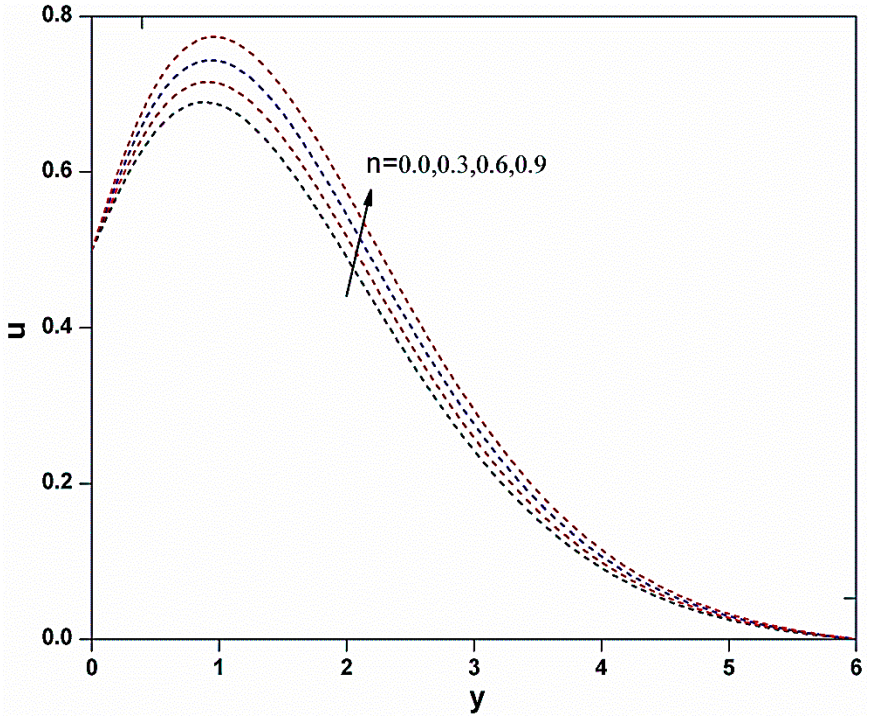

Figure 6: Velocity profiles for various values of n, when $t = 0.2, \beta = 0.5, \eta = 1.5, \alpha t = \pi/3$ $Gr = 5, Gm = 10, \Pr = 0.3, N = 3, Ec = 0.01, Sc = 0.2, \gamma = 1$.

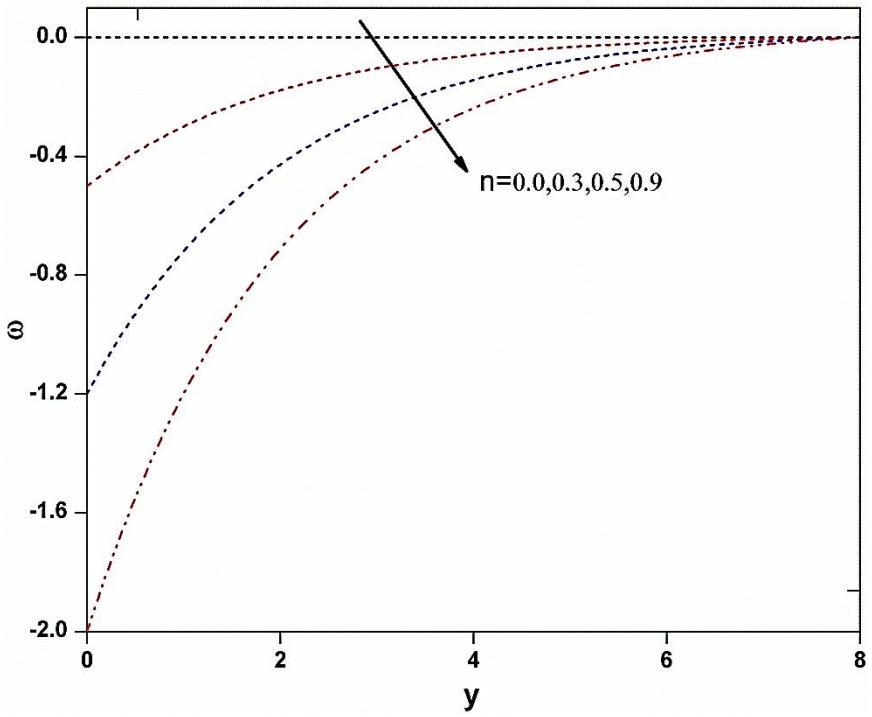

Figure 7: Micro-rotation for various values of n, when $t = 0.2, \beta = 0.5, \eta = 1.5, \alpha t = \pi / 3,$ $Gr = 5, Gm = 10, \Pr = 0.3, N = 3, Ec = 0.01, Sc = 0.2, \gamma = 1$

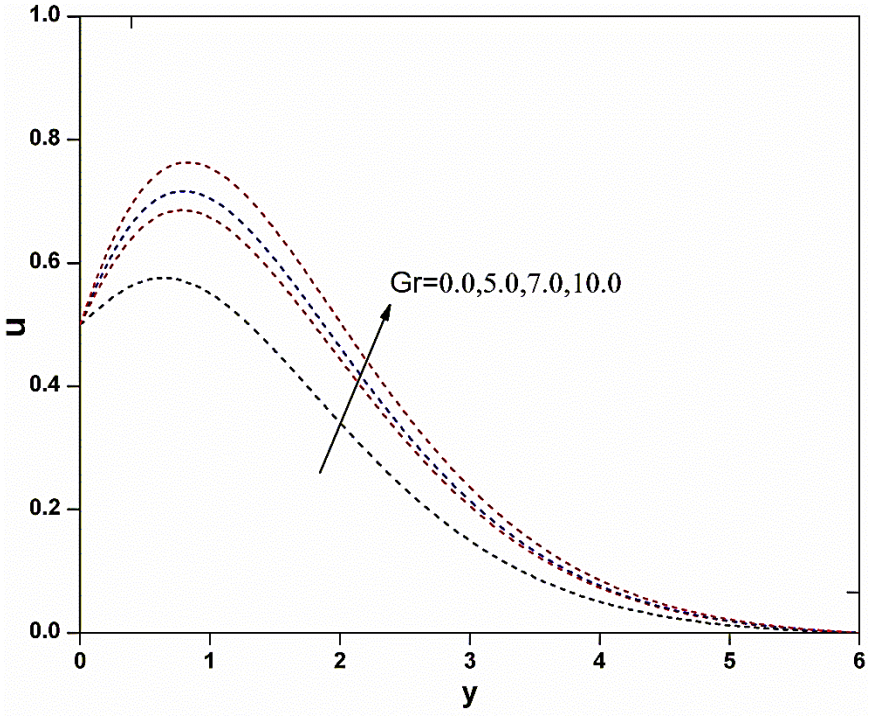

Figure 8: Velocity profiles for various values of Gr, when $t = 0.2, \beta = 0.5, \eta = 1.5, \alpha t = \pi / 3,$ $n = 0.6, Gm = 10, \Pr = 0.3, N = 3, Ec = 0.01, Sc = 0.2, \gamma = 1.$

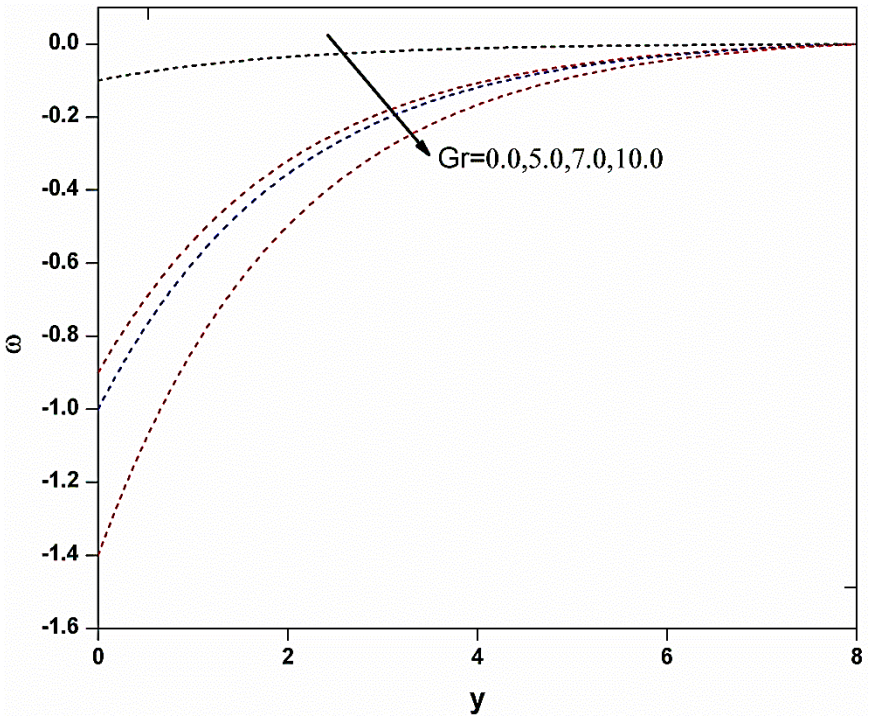

Figure 9: Micro-rotation for various values of Gr, when $t = 0.2, \beta = 0.5, \eta = 1.5, \alpha t = \pi/3$ $n = 0.6, Gm = 10, \Pr = 0.3, N = 3, Ec = 0.01, Sc = 0.2, \gamma = 1$.

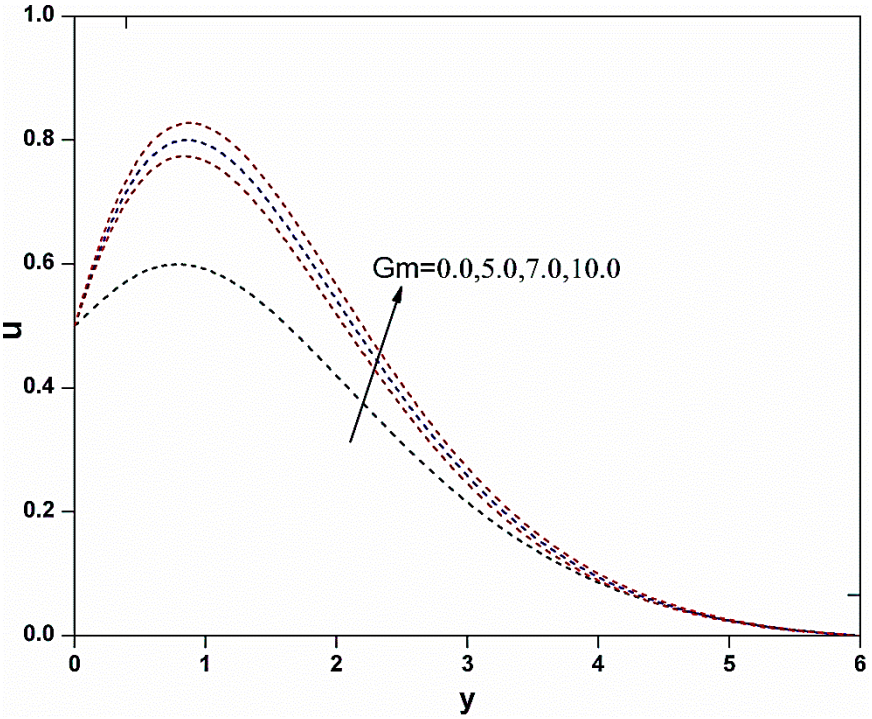

Figure 10: Velocity profiles for various values of Gm, when $t = 0.2, \beta = 0.5, \eta = 1.5, \alpha t = \pi/3$ $n = 0.6, Gr = 5, \Pr = 0.3, N = 3, Ec = 0.01, Sc = 0.2, \gamma = 1$.

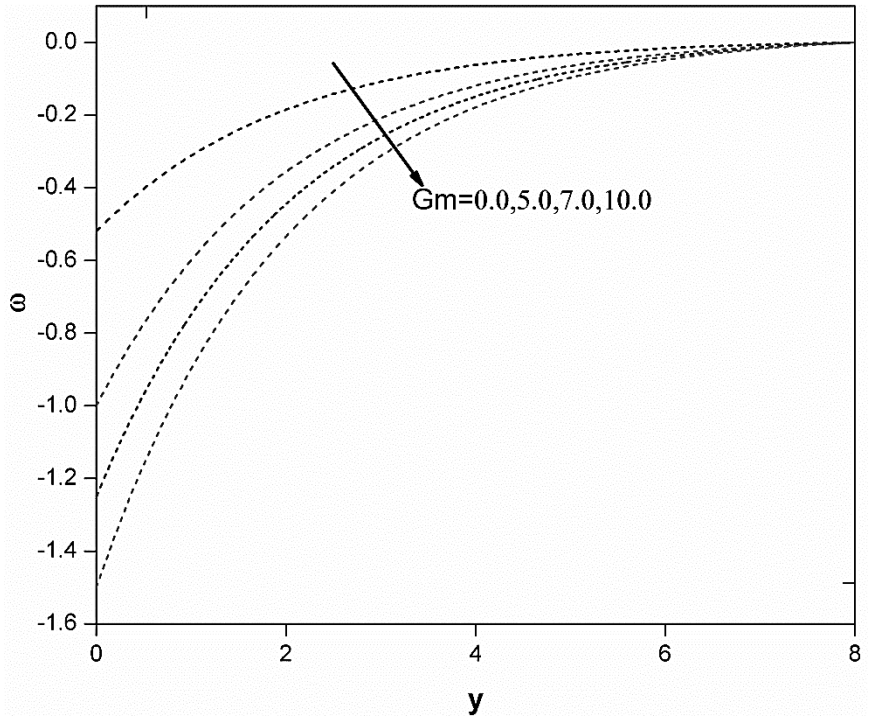

Figure 11: Micro-rotation for various values of Gm, when $t = 0.2, \beta = 0.5, \eta = 1.5, n = 0.6, \alpha t = \pi / 3, Gr = 5, \Pr = 0.3, N = 3, Ec = 0.01, Sc = 0.2, \gamma = 1$.

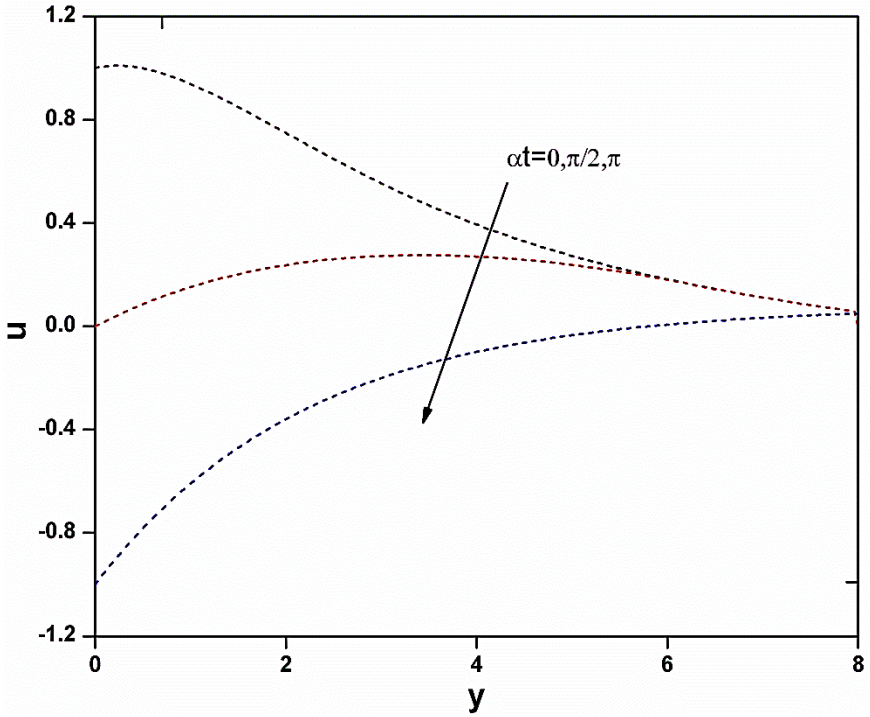

Figure 12: Velocity profiles for various values of αt, when $t = 0.2, \beta = 0.5, \eta = 1.5, n = 0.6, Gr = 5, Gm = 10, \Pr = 0.3, N = 3, Ec = 0.01, Sc = 1, \gamma = 1$.

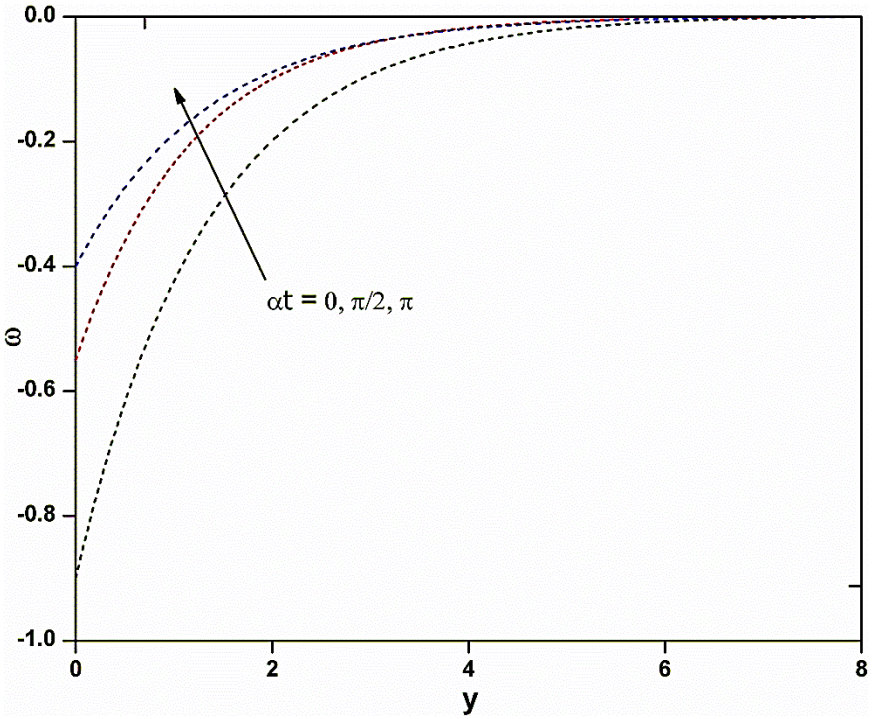

Figure 13: Micro-rotation profiles for various values of $\alpha\, t$, when $t = 0.2, \beta = 0.5, \eta = 1.5,$ $n = 0.6, Gr = 5, Gm = 10, \Pr = 0.3, N = 3, Ec = 0.01, Sc = 1, \gamma = 1.$

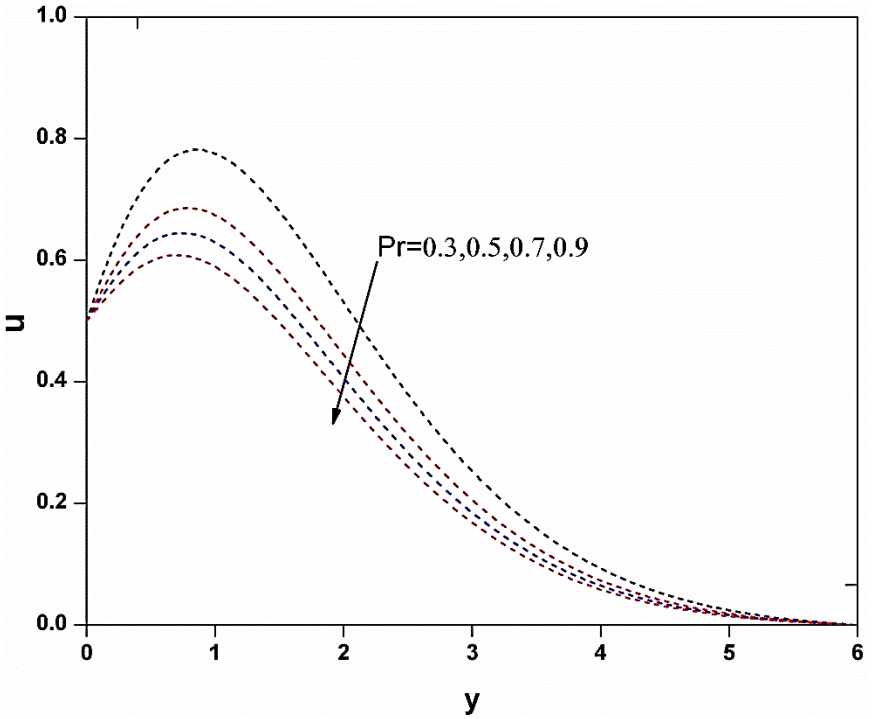

Figure 14: Velocity profiles for various values of $\Pr$, when $t = 0.2, \beta = 0.5, \eta = 1.5, n = 0.6,$ $\alpha t = \pi / 3, Gr = 5, Gm = 10, N = 3, Ec = 0.01, Sc = 0.2, \gamma = 1.$

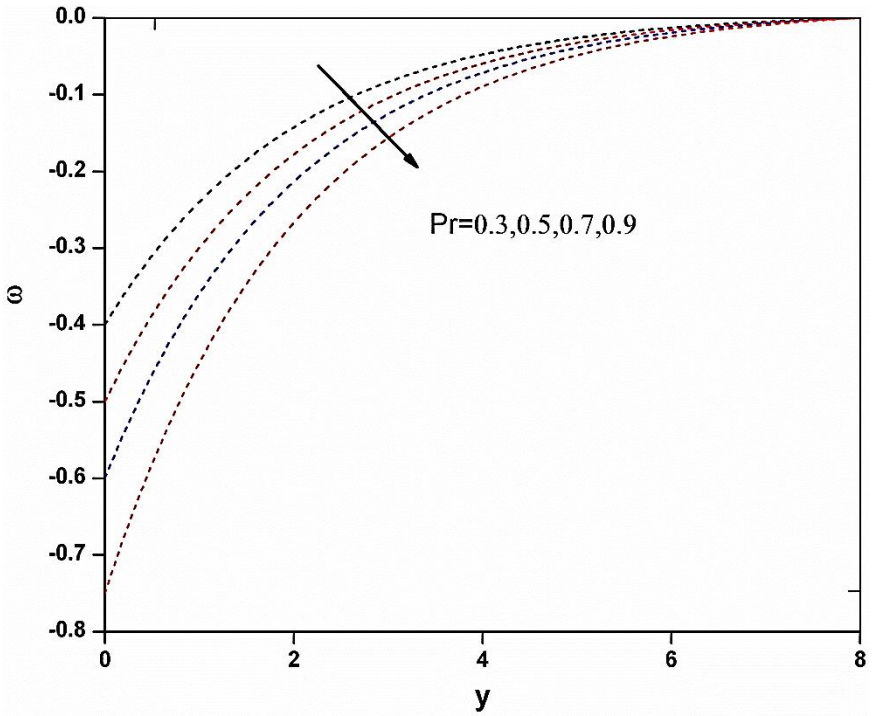

Figure 15: Micro-rotation for various values of Pr , when $t = 0.2, \beta = 0.5, \eta = 1.5, n = 0.6,$ $\alpha t = \pi / 3, Gr = 5, Gm = 10, N = 3, Ec = 0.01, Sc = 0.2, \gamma = 1.$

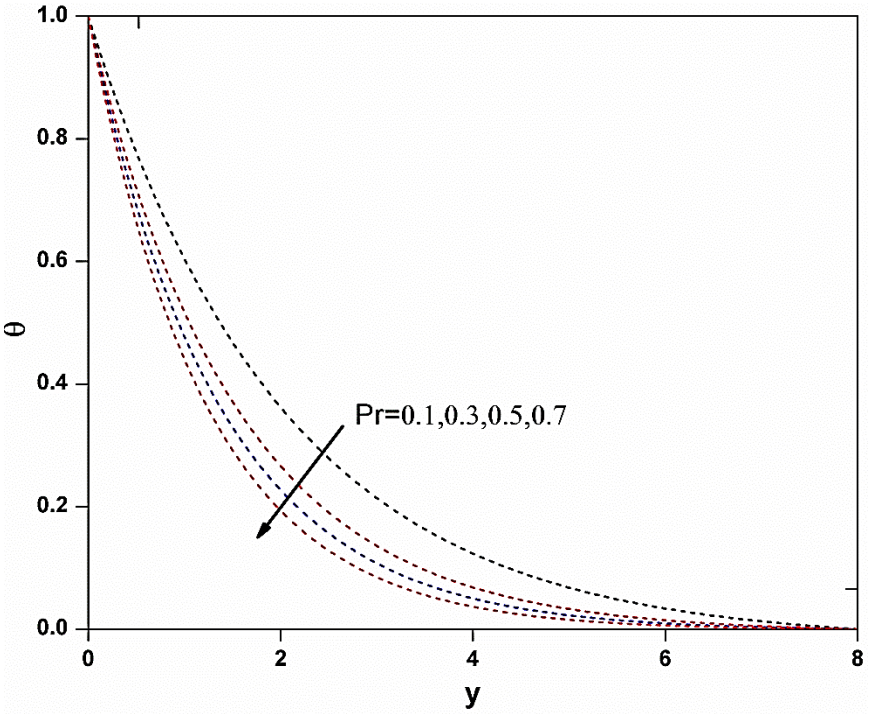

Figure 16: Temperature profiles for various values of Pr , when $t = 0.2, \beta = 0.5, \eta = 1.5, n = 0.6,$ $\alpha t = \pi / 3, Gr = 5, Gm = 10, N = 3, Ec = 0.01, Sc = 0.2, \gamma = 1.$

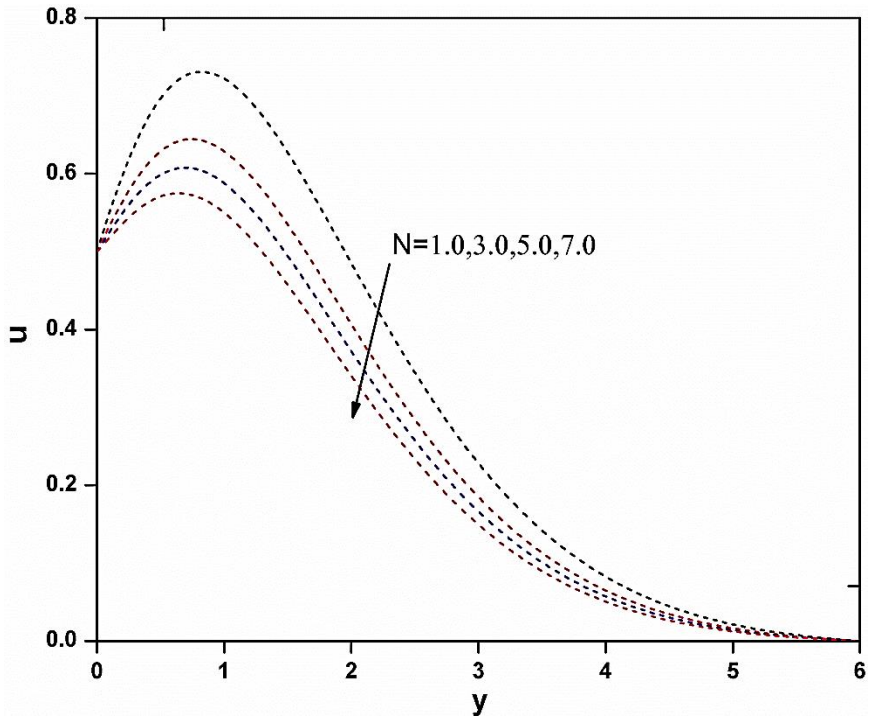

Figure 17: Velocity profiles for various values of N , when $t = 0.2, \beta = 0.5, \eta = 1.5, n = 0.6,$ $\alpha t = \pi / 3, Gr = 5, Gm = 10, Ec = 0.01, Sc = 0.2, \gamma = 1$.

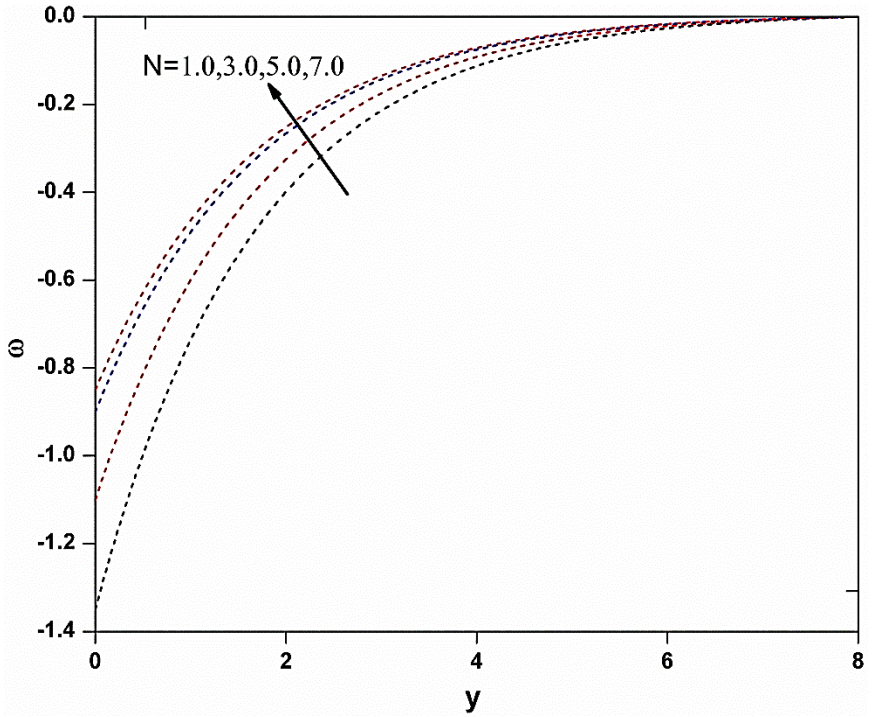

Figure 18: Micro-rotation for various values of N , when $t = 0.2, \beta = 0.5, \eta = 1.5, n = 0.6,$ $\alpha t = \pi / 3, Gr = 5, Gm = 10, Ec = 0.01, Sc = 0.2, \gamma = 1$.

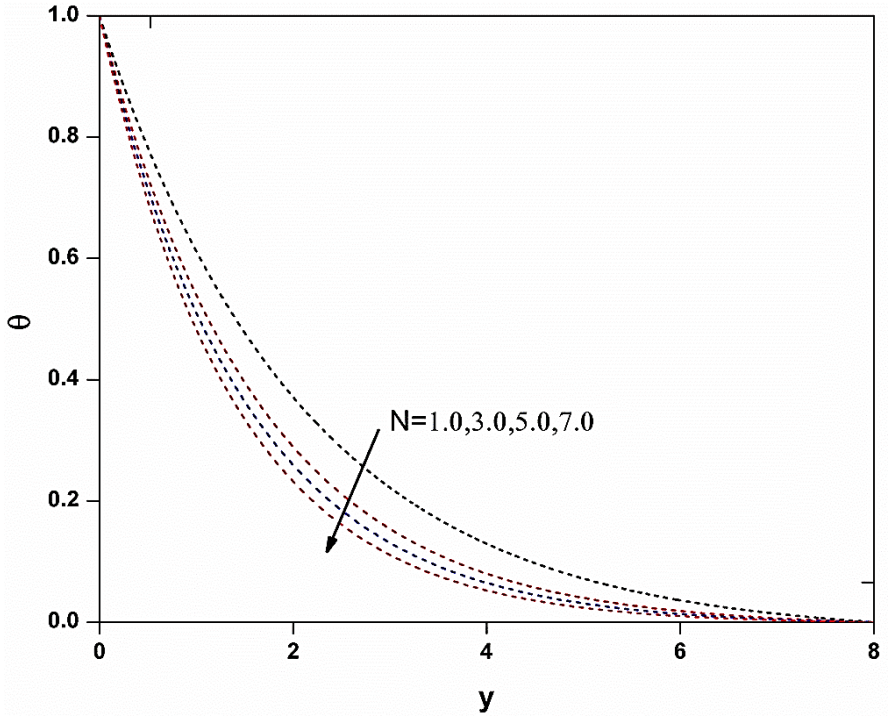

Figure 19: Temperature profiles for various values of N , when $t = 0.2, \beta = 0.5, \eta = 1.5, n = 0.6,$ $\alpha t = \pi / 3, Gr = 5, Gm = 10, Ec = 0.01, Sc = 0.2, \gamma = 1$.

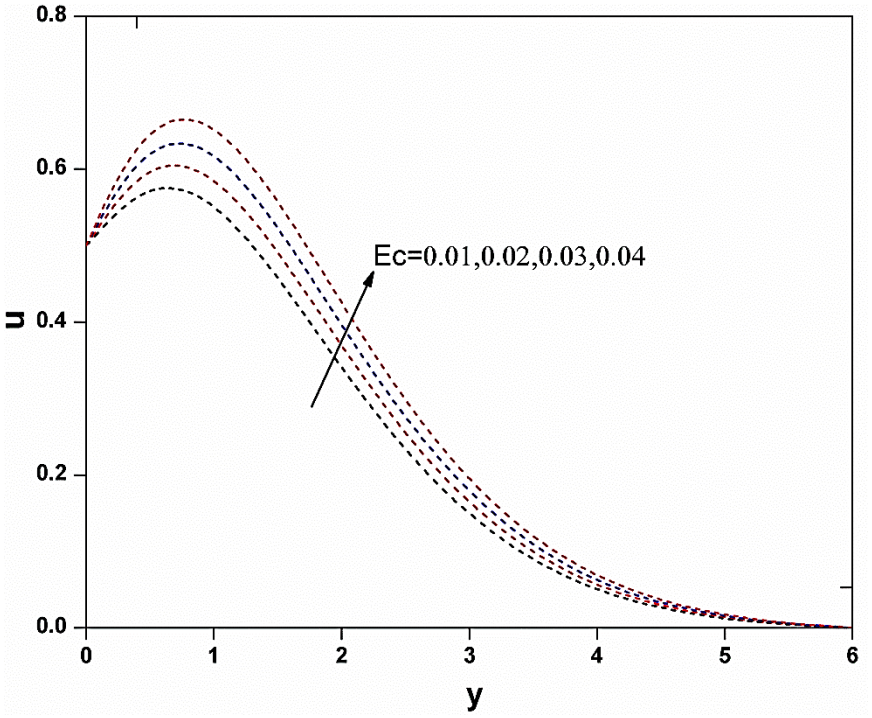

Figure 20: Velocity profiles for various values of Ec , when $t = 0.2, \beta = 0.5, \eta = 1.5, n = 0.6,$ $\alpha t = \pi / 3, Gr = 5, Gm = 10, N = 3, Sc = 0.2, \gamma = 1$.

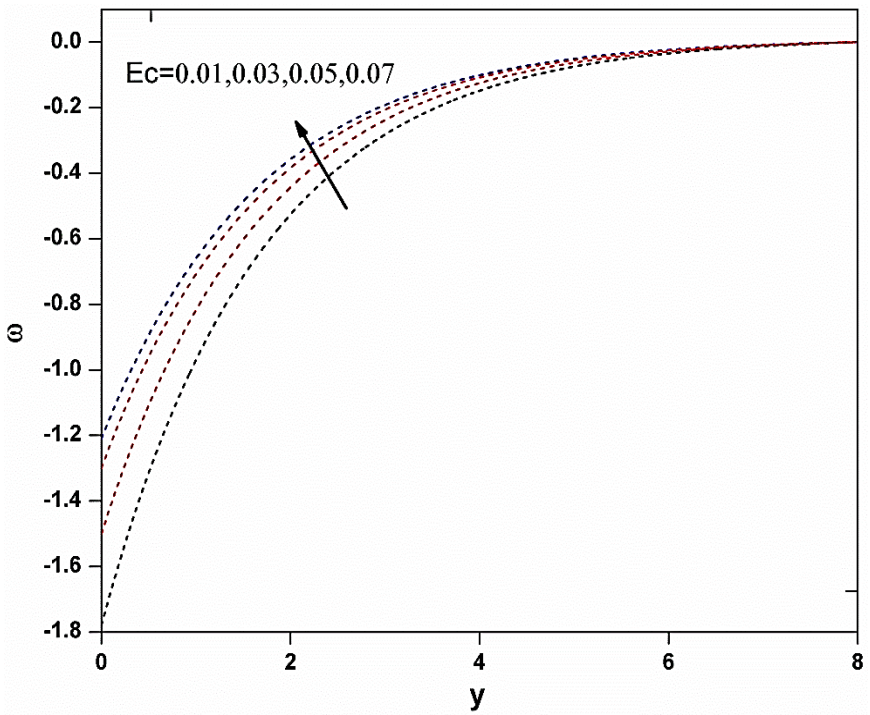

Figure 21: Micro-rotation for various values of Ec, when $t = 0.2, \beta = 0.5, \eta = 1.5, n = 0.6, \alpha t = \pi/3, Gr = 5, Gm = 10, N = 3, Sc = 0.2, \gamma = 1$.

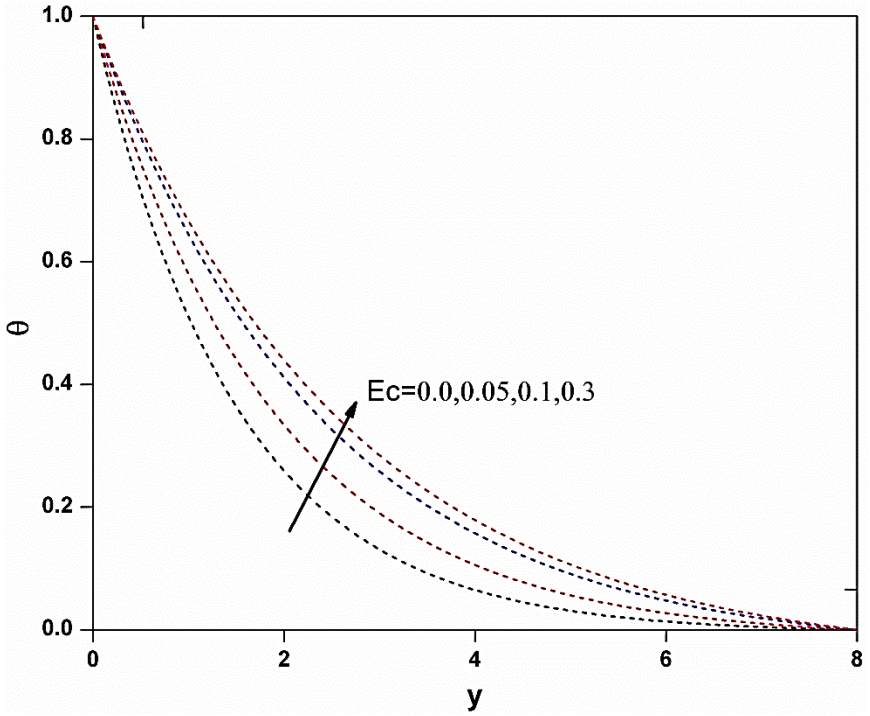

Figure 22: Temperature profiles for various values of Ec, when $t = 0.2, \beta = 0.5, \eta = 1.5, n = 0.6, \alpha t = \pi/3, Gr = 5, Gm = 10, N = 3, Sc = 0.2, \gamma = 1$.

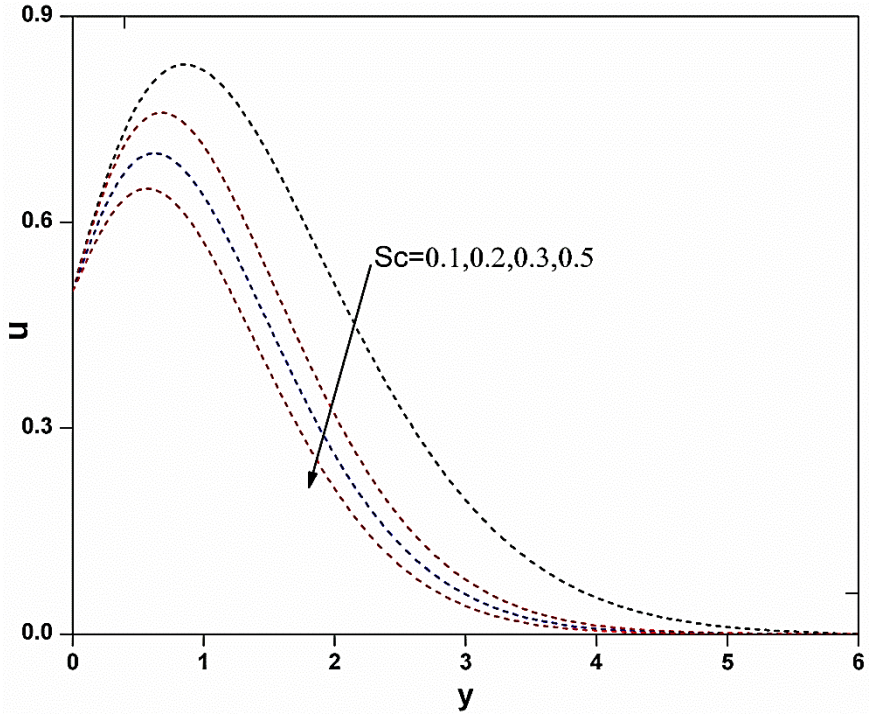

Figure 23: Velocity profiles for various values of Sc, when $t = 0.2, \beta = 0.5, \eta = 1.5, n = 0.6, \alpha t = \pi/3, Gr = 5, Gm = 10, N = 3, Ec = 0.01, \gamma = 1$.

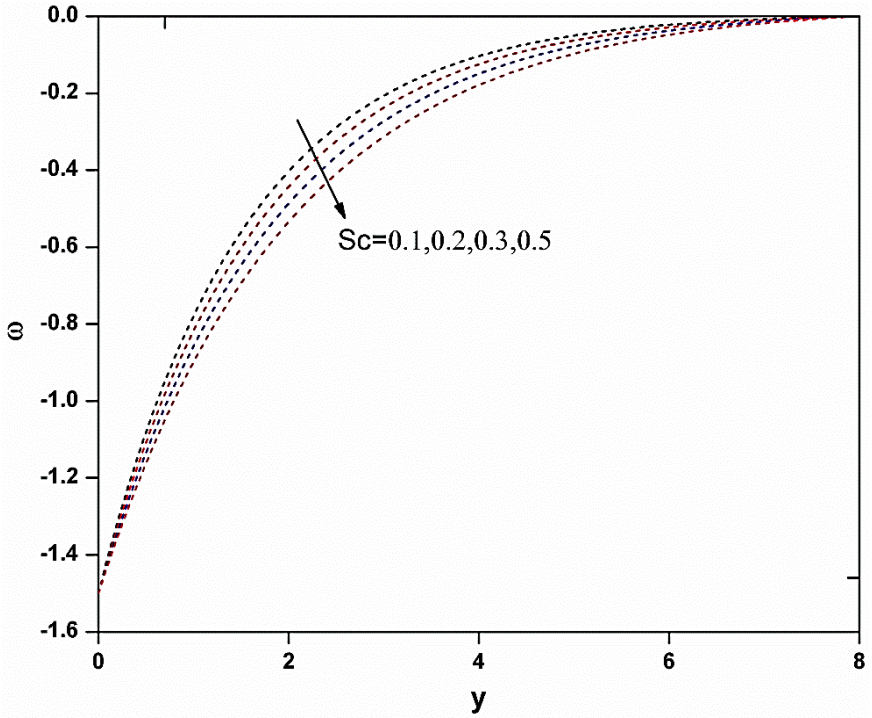

Figure 24: Micro-rotation for various values of Sc, when $t = 0.2, \beta = 0.5, \eta = 1.5, n = 0.6, \alpha t = \pi/3, Gr = 5, Gm = 10, N = 3, Ec = 0.01, \gamma = 1$.

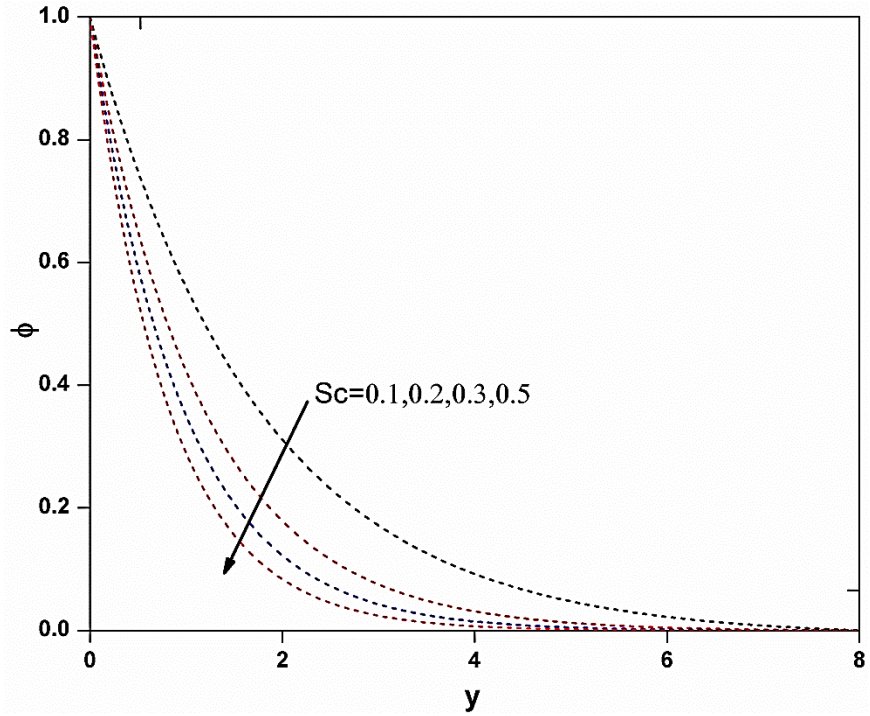

Figure 25: Concentration for various values of Sc, when $t = 0.2, \beta = 0.5, \eta = 1.5, n = 0.6, \alpha t = \pi/3, Gr = 5, Gm = 10, N = 3, Ec = 0.01, \gamma = 1$.

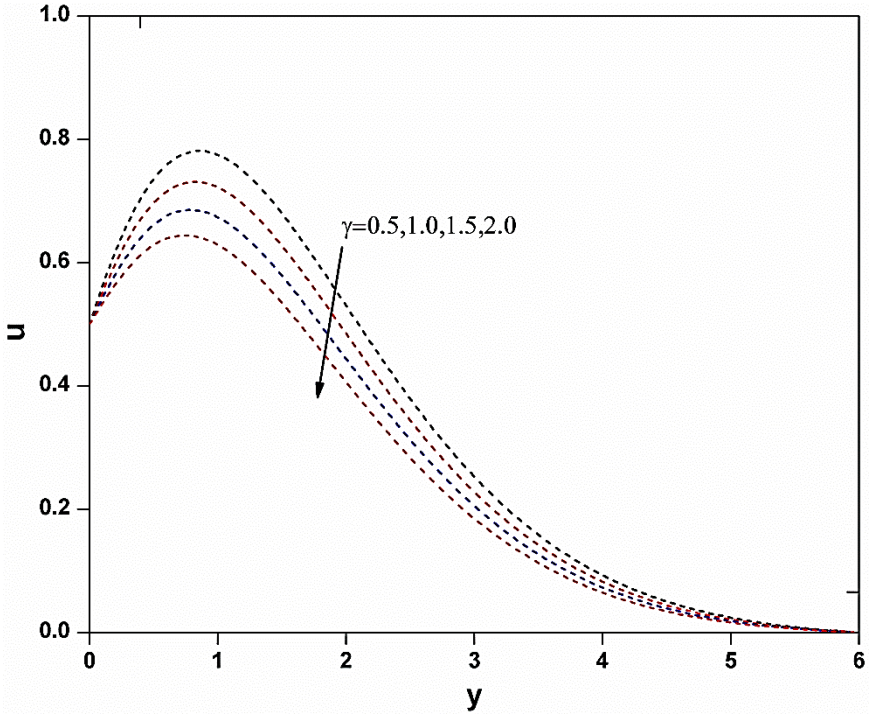

Figure 26: Velocity profiles for various values of γ, when $t = 0.2, \beta = 0.5, \eta = 1.5, n = 0.6, \alpha t = \pi/3, Gr = 5, Gm = 10, N = 3, Ec = 0.01, Sc = 0.2$.

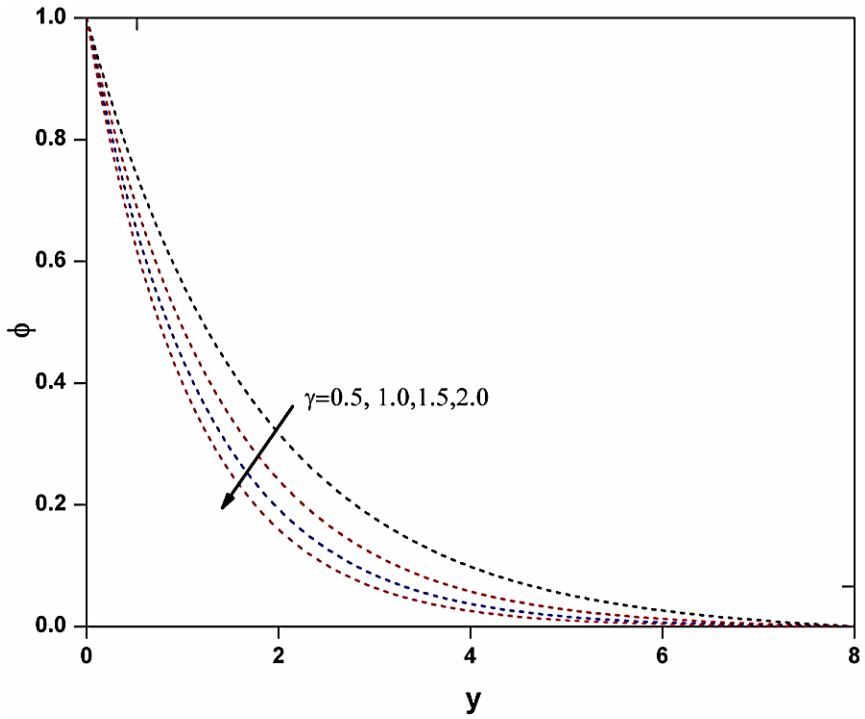

Figure 27: Concentration profiles for various values of γ , when $t = 0.2, \beta = 0.5, \eta = 1.5, n = 0.6,$ $\alpha t = \pi / 3, Gr = 5, Gm = 10, N = 3, Ec = 0.01, Sc = 0.2$.

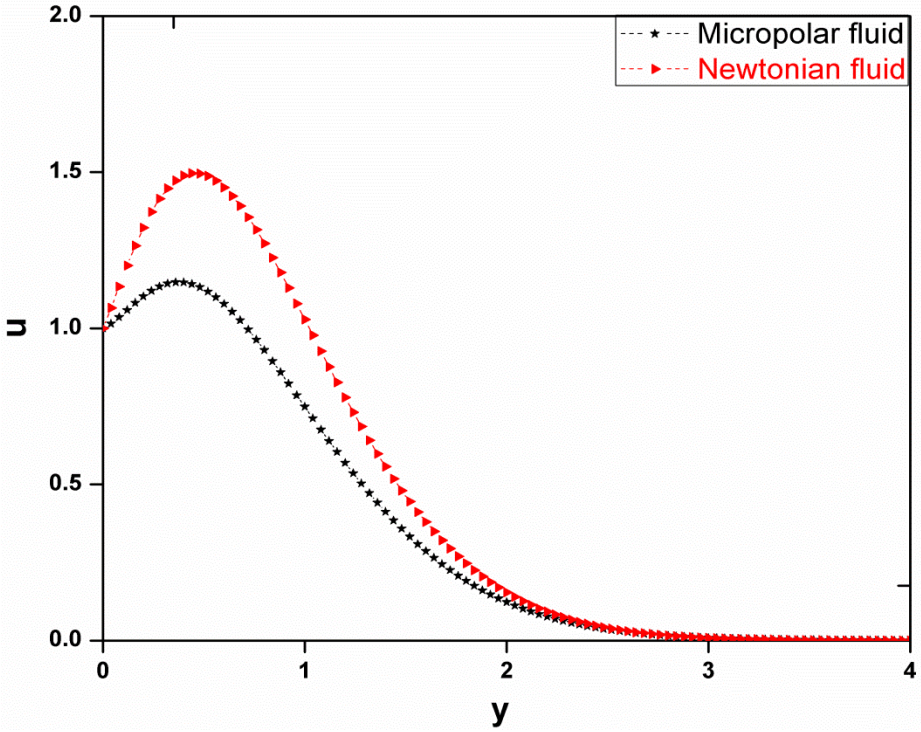

Figure 28: Comparison of micropolar fluid velocity (when $\beta = 1$), with Newtonian fluid velocity (when $\beta = 0$) and $\alpha t = 0$

Tables

Table 1. The numerical values of u, ω, θ and ϕ for different mesh (grid) sizes at $t = 0.2$

	Mesh size = 0.01				Mesh size = 0.001				Mesh size = 0.0001			
	u	ω	θ	ϕ	u	ω	θ	ϕ	u	ω	θ	ϕ
$t = 0.2$	**0.5000**	**-1.3500**	**1.0000**	**1.0000**	**0.5000**	**-1.3500**	**1.0000**	**1.0000**	**0.5000**	**-1.3500**	**1.0000**	**1.0000**
	0.5108	**-1.3177**	**0.9844**	**0.9819**	**0.5108**	**-1.3177**	**0.9844**	**0.9819**	**0.5108**	**-1.3177**	**0.9844**	**0.9819**
	0.5217	**-1.2862**	**0.9690**	**0.9641**	**0.5217**	**-1.2862**	**0.9690**	**0.9641**	**0.5217**	**-1.2862**	**0.9690**	**0.9641**
	0.5323	**-1.2554**	**0.9539**	**0.9466**	**0.5323**	**-1.2554**	**0.9539**	**0.9466**	**0.5323**	**-1.2554**	**0.9539**	**0.9466**
	0.5422	**-1.1961**	**0.9390**	**0.9295**	**0.5422**	**-1.1961**	**0.9390**	**0.9295**	**0.5422**	**-1.1961**	**0.9390**	**0.9295**
	0.5510	**-1.1674**	**0.9244**	**0.9127**	**0.5510**	**-1.1674**	**0.9244**	**0.9127**	**0.5510**	**-1.1674**	**0.9244**	**0.9127**
	0.5587	**-1.1395**	**0.9100**	**0.8961**	**0.5587**	**-1.1395**	**0.9100**	**0.8961**	**0.5587**	**-1.1395**	**0.9100**	**0.8961**
	0.5649	**-1.1122**	**0.8959**	**0.8799**	**0.5649**	**-1.1122**	**0.8959**	**0.8799**	**0.5649**	**-1.1122**	**0.8959**	**0.8799**
	0.5697	**-1.0856**	**0.8819**	**0.8640**	**0.5697**	**-1.0856**	**0.8819**	**0.8640**	**0.5697**	**-1.0856**	**0.8819**	**0.8640**
	0.5730	**-1.0342**	**0.8682**	**0.8483**	**0.5730**	**-1.0342**	**0.8682**	**0.8483**	**0.5730**	**-1.0342**	**0.8682**	**0.8483**
	0.5748	**-1.0094**	**0.8547**	**0.8329**	**0.5748**	**-1.0094**	**0.8547**	**0.8329**	**0.5748**	**-1.0094**	**0.8547**	**0.8329**

Table 2: Effects of β, n, Pr, Gr, Sc, Gm, αt, *and* t on C_f, C_m in the absence of N, Ec, and γ

								Khalid *et al.* [14]		Present results	
β	n	Pr	Gr	Gm	Sc	αt	t	C_f	C_m	C_f	C_m
0.5	0.6	0.3	5.0	5.0	0.2	$\pi/4$	0.6	3.2386	2.1322	3.238602	2.132215
2	0.6	0.3	5.0	5.0	0.2	$\pi/4$	0.6	3.3057	1.9754	3.305718	1.975408
0.5	**0.9**	0.3	5.0	5.0	0.2	$\pi/4$	0.6	2.5837	1.4587	2.583707	1.458719
0.5	0.6	**0.7**	5.0	5.0	0.2	$\pi/4$	0.6	3.4454	1.6312	3.445409	1.631202
0.5	0.6	0.3	**7.0**	5.0	0.2	$\pi/4$	0.6	2.0142	0.7485	2.014211	0.748507
0.5	0.6	0.3	5.0	**7.0**	0.2	$\pi/4$	0.6	2.6354	1.3651	2.635421	1.365116
0.5	0.6	0.3	5.0	5.0	**0.5**	$\pi/4$	0.6	3.5012	2.0392	3.501208	2.039202
0.5	0.6	0.3	5.0	5.0	0.2	$\pi/2$	0.6	3.4441	1.9929	3.444102	1.992904
0.5	0.6	0.3	5.0	5.0	0.2	$\pi/4$	**0.9**	2.9097	1.0834	2.909714	1.083421